Liquid-Crystal-Mediated Geometric Phase: From Transmissive to Broadband Reflective Planar Optics

Peng Chen, Bing-Yan Wei, Wei Hu,* and Yan-Qing Lu*

Planar optical elements that can manipulate the multidimensional physical parameters of light efficiently and compactly are highly sought after in modern optics and nanophotonics. In recent years, the geometric phase, induced by the photonic spin–orbit interaction, has attracted extensive attention for planar optics due to its powerful beam shaping capability. The geometric phase can usually be generated via inhomogeneous anisotropic materials, among which liquid crystals (LCs) have been a focus. Their pronounced optical properties and controllable and stimuli-responsive self-assembly behavior introduce new possibilities for LCs beyond traditional panel displays. Recent advances in LC-mediated geometric phase planar optics are briefly reviewed. First, several recently developed photopatterning techniques are presented, enabling the accurate fabrication of complicated LC microstructures. Subsequently, nematic LC-based transmissive planar optical elements and chiral LC-based broadband reflective elements are reviewed systematically. Versatile functionalities are revealed, from conventional beam steering and focusing, to advanced structuring. Combining the geometric phase with structured LC materials offers a satisfactory platform for planar optics with desired functionalities and drastically extends exceptional applications of ordered soft matter. Some prospects on this rapidly advancing field are also provided.

1. Introduction

The flexible modulation and engineering of multiple degrees of freedom (e.g., wavelength/frequency, amplitude, polarization, and phase) of light lie at the heart of optics.[1] Traditional optical devices are based on the refraction, reflection, or diffraction of light, and they always rely on the phase accumulation along the propagation in an optical medium with a fixed refractive index (e.g., fused silica and photoresist), known as the "dynamic phase." Spatially curved surfaces are usually inevitable, resulting in a bulky size, large weight, and precisely controlled and time-consuming fabrication process, especially for complex wavefront tailoring. Along with the increasing requirements of the data-storage capacity and information-processing speed in modern science and technology, planar optical devices with a compact volume and multifunctional performances are in ever-growing demand.[2,3] Over the past decade, impressive progress has been achieved in research on the so-called "geometric phase," also referred to as "Pancharatnam–Berry phase."[4] Unlike the aforementioned dynamic phase that arises from optical path differences, the geometric phase originates from the spin–orbit interaction (SOI) of light[5] and describes the relationship between the phase change and the polarization conversion when the light is transmitted through an anisotropic medium. The magnitude of the geometric phase is usually proportional to the orientation angle of the effective local optical axis and has a polarization-dependent sign. Therefore, it only depends on the geometrical characteristics, regardless of any phase retardance condition or material dispersion, making corresponding optical elements flat, physically thin, and robust against fabrication tolerances.[6] The geometric phase provides an effective way for the miniaturization and integration of optical devices, and it has become a valuable candidate for functional planar optics.[7]

The geometric phase can be obtained in inhomogeneous anisotropic media, the most representative of which are metasurfaces[2,8] and liquid crystals (LCs).[9–11] Geometric metasurfaces are planar metamaterials consisting of anisotropic, subwavelength metallic/dielectric antennas with identical geometric parameters but spatially variant orientations arranged in 2D interfaces. These artificial scatterers with specially designed orientations, such as nanorods, nanoslits, and C-/L-/U-shaped split-ring resonators, have been developed to precisely modify the fundamental dimensions of light on an ultrahigh resolution and deep subwavelength scale, supplying extraordinary functionalities that are unachievable by ordinary diffractive

Dr. P. Chen, Prof. W. Hu, Prof. Y.-Q. Lu
National Laboratory of Solid State Microstructures
Key Laboratory of Intelligent Optical Sensing and Manipulation
College of Engineering and Applied Sciences
and Collaborative Innovation Center of Advanced Microstructures
Nanjing University
Nanjing 210093, China
E-mail: huwei@nju.edu.cn; yqlu@nju.edu.cn
Prof. B.-Y. Wei
MOE Key Laboratory of Material Physics and Chemistry under
Extraordinary Conditions
and Shaanxi Key Laboratory of Optical Information Technology
School of Science
Northwestern Polytechnical University
Xi'an 710072, China
Prof. W. Hu
Institute for Smart Liquid Crystals
JITRI
Changshu 215500, China

**ADVANCED
SCIENCE NEWS**

www.advancedsciencenews.com

**ADVANCED
MATERIALS**

www.advmat.de

optics.[12] Via such ultracompact geometric metasurfaces, arbitrary wavefront engineering can be realized, such as spin-controlled focus/defocus, diffraction, vortex/vector beam generation, and helicity multiplexed holograms.[8,13] Despite such impressive progress, some challenging issues persist, especially in decreasing the fabrication cost, improving the optical efficiency, and achieving dynamic tunability. In this respect, LCs have unique superiorities and irreplaceable capabilities.

LC is a natural state of matter between liquid and crystalline materials, featuring both the fluidity of liquid and the optical/dielectric anisotropy of crystals. In general, LCs can be categorized as various mesophases, such as the traditional nematic, chiral cholesteric, and lamellar smectic, as shown respectively in **Figure 1**.[14] LC molecules are typically anisotropic in shape and self-assemble with a preferred direction of orientation, namely, the local director n (i.e., local optical axis).[15] A variety of remarkable properties are exhibited: the pronounced large birefringence and high transparency over a wide electromagnetic spectrum; controllable and reconfigurable space-variant director orientation; high sensibility to surface chemistry, confined geometry, and various external field stimuli (e.g., electric/magnetic field, light irradiation, and heat); strong capability for matter and electromagnetic field interactions.[16,17] As an excellent electro-optical material, LC has become one of the most attractive candidates for the development of tunable optical devices. In particular, its reliability has been well proven in information displays. Currently, the liquid crystal display (LCD) retains a dominant position in the panel display market, which can be considered a practical example for intensity modulation of visible light.[18] In recent years, LC structuring techniques have been rapidly developed, inspiring the free manipulation of other spatial degrees of light. Patterned electrodes (typically the commercial spatial light modulator, SLM),[1,19] polymer dispersion,[20] and microrubbing[21,22] have been adopted to generate distinguished LC patterns and structures successively. Compared with these methods, photoalignment is much more suitable for implementing high-resolution multidomain LC alignments.[23–25] In initial research, multistep photolithography[24] and holography[26,27] were commonly utilized. More recently, several innovative technologies exhibiting superior flexibility have been exploited,[10,28–31] facilitating the realization of complex LC microstructures and improving the subsequent optical performances. The collaboration of the "top-down" photopatterning process and "bottom-up" self-assembly promotes the control of LC superstructures on an unprecedented level, providing new possibilities for LCs, particularly in geometric phase optics.

The past few years have witnessed enormous progress in LC-mediated geometric phase planar optics. In early days, the main efforts were devoted to the creation and optimization of the nematic LC-based geometric phase,[10,11] which has shown significant advantages in many practical applications. Very recently, the chiral LC (CLC) superstructures have also been discovered to possess unique features of polychromatic and spin-determined reflective geometric phase modulation.[32–34] Benefitting from the intrinsic rapid self-organization and external-stimuli response of these soft chiral materials,[35–37] it immediately becomes an emerging frontier and opens a new door toward active and multifunctional planar optics. Here, we will

Peng Chen obtained his B.S. and Ph.D. degrees in material physics and optical engineering from Nanjing University, China, in 2014 and 2019, respectively. He is currently a research associate in the group of Prof. Yan-Qing Lu at the College of Engineering and Applied Sciences at Nanjing University. His research interests focus on nanostructured liquid crystals and the corresponding optical applications.

Wei Hu earned his Ph.D. degree in polymer chemistry from Jilin University, China, in 2009. He is now a Tang Scholar and professor of optical engineering in Nanjing University, China. His research fields are liquid crystal materials and optical devices, with a focus on photoalignment-enabled liquid crystalline hierarchical architectures, optically addressed spatial light modulators, and liquid crystal telecom/terahertz elements.

Yan-Qing Lu received both his B.S. and Ph.D. degrees from Nanjing University, China, in 1991 and 1996, respectively. He has five years of experience in telecom industries in the United States and China. He is currently a Changjiang distinguished professor at Nanjing University and a fellow of the Optical Society of America and Chinese Optical Society. His research interests include liquid crystal photonics, fiber optics, and nonlinear optics.

mainly concentrate on the recent advances of the LC-mediated geometric phase. We begin with a brief introduction to the concept and principle of the geometric phase. Then, various powerful photopatterning techniques capable of accurately fabricating arbitrary LC microstructures are introduced. Nematic LC-based transmissive and chiral LC-based broadband reflective planar optics are subsequently discussed in detail. Numerous spin-controlled functionalities are revealed, from conventional beam steering and focusing, to advanced structuring of light. Finally, this short review is summarized with a comment on
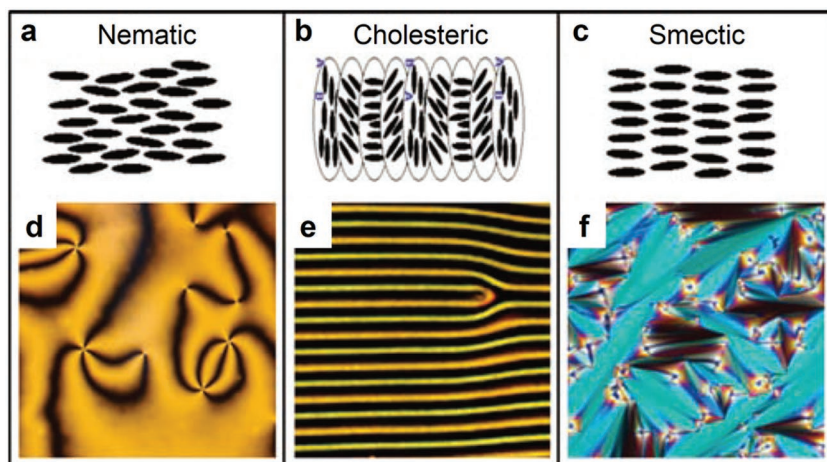
ADVANCED
SCIENCE NEWS
www.advancedsciencenews.com

ADVANCED
MATERIALS
www.advmat.de

Figure 1. Schematics of the molecular structures and corresponding textures of three typical LC mesophases. a) Nematic LC with d) point defects, b) cholesteric LC with a e) fingerprint texture, and c) smectic LC with a f) fan-shaped focal conic texture. Reproduced with permission.[14] Copyright 2011, Wiley-VCH.

the current research status and an outlook regarding potential future prospects in this rapidly growing area.

2. Geometric Phase of Light

In the context of optics, the theoretical maximum diffraction efficiency of the first order is 40.5% for binary optics.[38] To further improve the efficiency for light control, a continuous phase variation covering 0 to 2π should be extracted to suppress higher diffraction orders. If using normal optical isotropic materials based on the principle of the dynamic phase, then a continuously variant optical path difference should be guaranteed, that is, a smooth change in thickness, which is certainly harmful for the miniaturization and integration of optical devices. In contrast, the geometric phase supplies a compact and versatile strategy. The geometric phase is strictly related to the space-variant transformation of the light polarization states, and it is independent of the optical path length. It is the manifestation of the SOI of light, which is a novel electromagnetic effect that describes the interplay between the photon spin (i.e., the handedness of circular polarization) and the trajectory of light.[5] The spin can affect and control the spatial degrees of freedom of light, such as the intensity profile and the propagation direction. Properly designing anisotropic and inhomogeneous structures allows considerable enhancement of the SOI effects and high-efficiency spin-determined control of light, in particular spin-dependent light splitting (namely, the photonic spin Hall effect)[39,40] and spin-to-orbital angular momentum conversion.[9,41] Spin and orbital angular momenta are the intrinsic freedoms of light, which add a brand new way to manipulate light and drastically extend the capacity of optical communication systems.

The geometric phase can be acquired from the interplay between the polarization states. For two light beams with the same initial polarization state, if they experience different variations to reach the same terminal polarization while propagating along the same distance, there would exist a phase difference

between them, which is the geometric phase. From the description on the Poincaré sphere, the same initial and terminal polarization states correspond to the identical two points on the surface, and different polarization variations indicate distinct routes between these two points. The induced geometric phase can be deduced as the half of the solid angle Ω enclosed by corresponding traces on the Poincaré sphere.[17,40] As an example shown in **Figure 2**a, two routes start at the north pole, which represents the right circular polarization (RCP), and then pass through different points on the equator indicating two linear polarizations with different directions (0° and 45°) and end at the south pole, which represents the left circular polarization (LCP). Accordingly, the enclosed solid angle is $\Omega = \pi$, and thus the geometric phase difference is $\pi/2$. Therefore, by controlling local polarization conversions, the light phase-front can be feasibly tailored, which has currently been attracting growing attention.

Anisotropic optical materials are necessary to efficiently manipulate the polarization of light. To implement geometric phase modulation, the spatially varying anisotropy in the 2D plane should be obtained. As a natural birefringent material, LCs satisfy those requirements and exhibit versatile capabilities. The geometric phase can be theoretically predicted through Jones matrix calculation. Considering an inhomogeneous LC waveplate with the distribution of a local optical axis (i.e., nematic LC director) following $\alpha(x, y)$ in the x–y plane, under the normal incidence, its Jones matrix can be expressed as follows[17]

$$\mathbf{J} = \mathbf{R}(-\alpha) \cdot \begin{bmatrix} \exp(-i\Gamma/2) & 0 \\ 0 & \exp(i\Gamma/2) \end{bmatrix} \cdot \mathbf{R}(\alpha)$$
$$= \cos\frac{\Gamma}{2}\mathbf{I} - i\sin\frac{\Gamma}{2}\begin{bmatrix} \cos(2\alpha) & \sin(2\alpha) \\ \sin(2\alpha) & -\cos(2\alpha) \end{bmatrix} \tag{1}$$

where $\mathbf{R}$ is the rotation matrix and $\mathbf{I}$ is the identity matrix. Γ is the phase retardation resulting from the birefringence of LCs, which can be given by the following

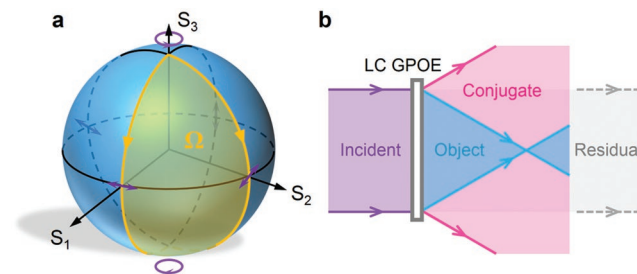$$\Gamma = \frac{2\pi(n_{\text{eff}} - n_{\text{o}})d}{\lambda} \tag{2}$$

Figure 2. a) Schematic illustration of the geometric phase by different traces on the Poincaré sphere, which results in a phase change equaling $\Omega/2$. b) Schematic diagram of the nematic LC-mediated transmissive geometric phase optical element (GPOE) and its diffraction property. Reproduced with permission.[10] Copyright 2015, Optical Society of America.

**ADVANCED
SCIENCE NEWS**

www.advancedsciencenews.com

**ADVANCED
MATERIALS**

www.advmat.de

where d is the LC cell gap, λ is the free-space wavelength of incident light, n_o is the ordinary refractive index, and n_{eff} is the effective extraordinary refractive index that changes gradually from n_e to n_o according to the tilting of the LC director.[15] Considering a circularly polarized incident light, it can be described as $\mathbf{E}_{in} = \frac{1}{\sqrt{2}}\begin{pmatrix} 1 \\ \pm i \end{pmatrix} = \chi^{(\pm)}$, with two spin eigenstates $|L\rangle = \frac{1}{\sqrt{2}}\begin{pmatrix} 1 \\ +i \end{pmatrix}$ and $|R\rangle = \frac{1}{\sqrt{2}}\begin{pmatrix} 1 \\ -i \end{pmatrix}$ corresponding to LCP and RCP states, respectively. After passing through the LC wave-plate, the output light can be written as follows

$$\mathbf{E}_{out} = \mathbf{J} \cdot \mathbf{E}_{in} = \cos\frac{\Gamma}{2}\mathbf{E}_{in} - i\sin\frac{\Gamma}{2}e^{\pm i2\alpha}\chi^{(\mp)} \tag{3}$$

where $\pm 2\alpha$ is the geometric phase induced in this light–matter interaction process.

As clearly shown in Figure 2b, the first term in Equation (3) is the residual light component with the same helicity and wavefront as incident light, while the second term represents the transformed one with an opposite helicity and an additional geometric phase of $\pm 2\alpha$, with the + sign for conversion from LCP to RCP and the – sign for RCP to LCP. Therefore, as the LC director is rotated from 0° to 180°, a continuous phase change over the full phase range from 0 to 2π can be added to the converted component with orthogonal circular polarization. Thus, by encoding half of the desired phase function into the in-plane distribution of LC directors, arbitrary phase shaping can be achieved with spin-dependent phase conjugation. On the other hand, the phase retardation Γ determines the intensity ratio among the residual and transformed components. The corresponding transformation efficiency is as follows

$$\eta_T = \sin^2\frac{\Gamma}{2} \tag{4}$$

Especially, when the half-wave condition is satisfied, i.e., $\Gamma = (2a + 1)\pi$ (a is an integer), only the second term in Equation (3) exists, and the incident light will be completely transformed to a desired phase profile ($\eta_T = 1$, ON state). In this case, the emerging light for LCP and RCP can be expressed as follows

$$\mathbf{J}|L\rangle = |R\rangle e^{+i2\alpha} \text{ and } \mathbf{J}|R\rangle = |L\rangle e^{-i2\alpha} \tag{5}$$

Usually, the LC-mediated geometric phase optical elements (GPOEs) work in this state by particularly choosing the refractive indices of LCs, optimizing the cell gap, or applying specific external fields. In contrast, for the full-wave condition, i.e., $\Gamma = 2a\pi$, there is only the first term, and the geometric phase effect is completely suppressed ($\eta_T = 0$, OFF state). Due to the excellent electro-optical tunability of LC materials, it is possible to dynamically switch between ON and OFF states and achieve equivalent high efficiencies at different wavelengths by slightly tuning the applied voltages.

3. LC Photopatterning System

To carry out the desired continuously variant LC directors, patterning technology is the key. In early days, a traditional rubbing method was adopted to align the polyimide, forming the

circular-symmetric geometry.[9,21,42] However, this method is only suitable for certain specific elements. Fortunately, more complicated LC microstructures can be further achieved via photoalignment technology. Compared with the conventional contact rubbing technique, photoalignment is superior for high-quality and high-resolution multidomain orientation LCs.[24,25,43–45] The noncontact photoalignment technology can avoid any mechanical damage, electrostatic charge, or dust contamination, and it is also available for curved or flexible substrates. It results from the anisotropic intermolecular interactions between the alignment agent and adjacent LC molecules. According to the respective mechanisms, the photoalignment agents can be divided into different types.[25] Take the widely used SD1[46] for example. As shown in **Figure 3**, because of their photoisomerization and dichroic absorption, the sulfonic azo-dye SD1 molecules tend to reorient their absorption oscillators perpendicular to the polarization direction of the illuminated UV light.[47] SD1 will further orient LC molecules with an anchoring energy larger
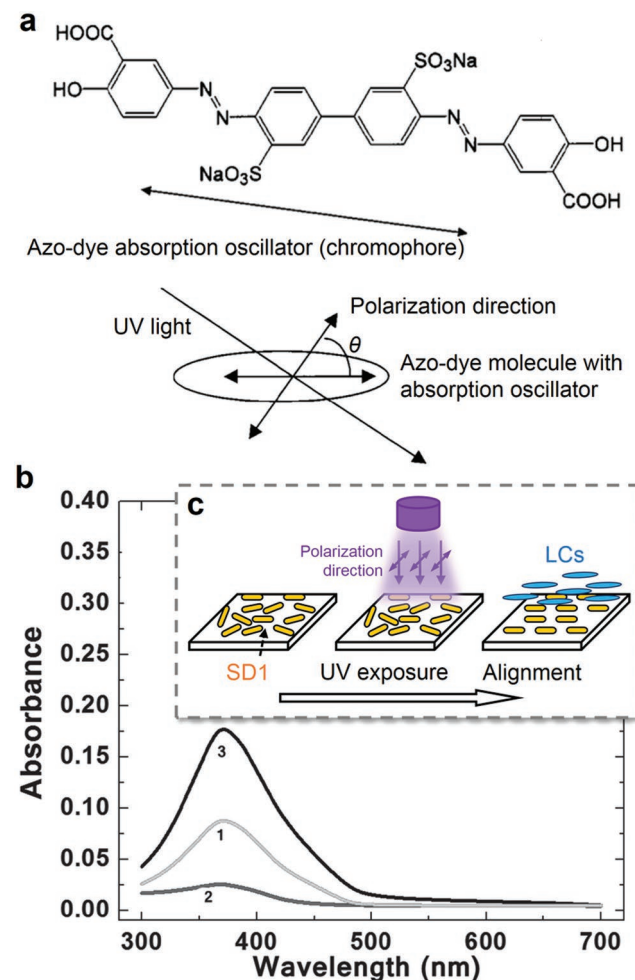

Figure 3. a) Chemical structure and diffusion model of the sulfonic azo-dye SD1. Reproduced with permission.[46] Copyright 2002, Taylor & Francis. b) Absorption spectra of SD1 before exposure to polarized UV light (curve 1) and after exposure to UV light polarized in the direction parallel (curve 2) and perpendicular (curve 3) to the polarization of activating light. Reproduced with permission.[73b] Copyright 2015, Wiley-VCH. c) Diagram of the photoalignment process based on SD1.

than 10^{-4} J cm^{-2}, which is comparable to that of the rubbed polyimide layer. Therefore, the director distributions of LC GPOEs can be conveniently achieved through UV exposure with spatially varying linear polarizations. It is worth mentioning that the SD1 is rewritable and could be reoriented by UV light, which restricts its applications in corresponding wavelength range. This issue could be satisfactorily addressed by introducing inerasable alignment agents or LC polymers.

During the past few years, several photopatterning systems have been developed, facilitating the fabrication of LC GPOEs.[48] At first, a rotating system, comprising mainly an angular/line mask, a polarizer, and a cylindrical lens, was adopted to fabricate the circular-symmetric LC alignment.[49–52] To achieve arbitrary LC patterns, Guo et al. proposed an engineered plasmonic metamask (PMM),[30,53] which is an effective tool for forming a spatially variant polarization distribution of the exposure light. Due to the extraordinary optical transmission, an unpolarized UV light passing through the rectan-

gular nanoaperture[30] or parallelepiped[54] units of the aluminum PMM exhibits local linear polarization with a direction that is perpendicular to the long axis of corresponding unit. **Figure 4**a depicts the PMM-based single-exposure photopatterning system. After the high-power light source illuminates the PMMs, the transmitted light carries the polarization fields consistent with mask patterns, is collected by the imaging objective and then coupled to the back aperture of the projection objective, and finally focused onto the LC cells. A tube lens and a charge coupled device (CCD) are utilized to inspect the focusing of the patterns. A much higher spatial resolution going beyond the Rayleigh criteria can be obtained by this plasmonic photopatterning.[55] Similarly, LC polymer films were applied by Tam et al. as polarization masks,[56] which exhibited high transmission in the visible spectrum and good thermal and photochemical stability. As illustrated in Figure 4b, the setup consists of a linear polarizer, a quarter-wave plate (QWP), and two LC polymer elements, enabling the photopatterning of
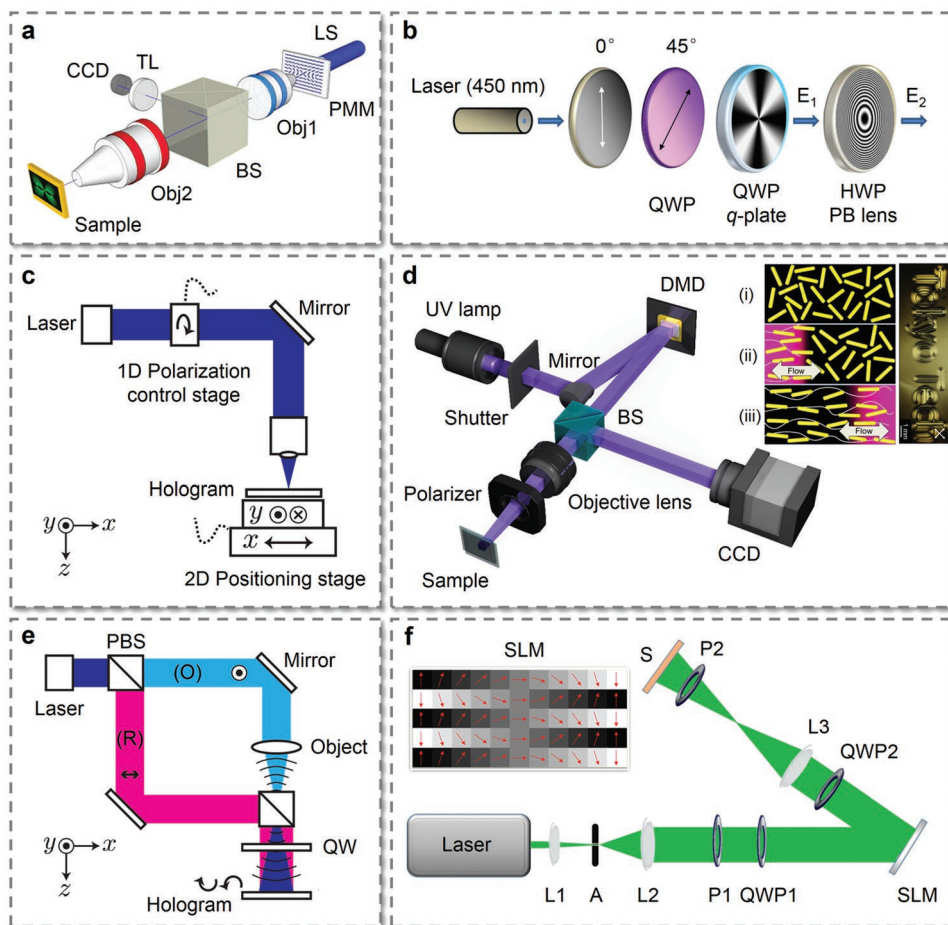

Figure 4. Different LC photopatterning systems. a) With metamasks. LS: light source; Obj1: imaging objective; BS: beam splitter; Obj2: projection objective; TL: tube lens. Reproduced with permission.[30] Copyright 2016, Wiley-VCH. b) With LC polymer masks. Reproduced with permission.[56] Copyright 2017, American Physical Society. c) Direct-writing and e) interference mask-free photopatterning systems. Reproduced with permission.[10] Copyright 2015, Optical Society of America. d) DMD-based dynamic mask photopatterning system. Reproduced with permission.[102a] Copyright 2016, Nature Publishing Group. Insets: schematic illustrations of the scanning wave photopolymerization (SWaP) process and micrograph of the patterned words "Tokyo Tech." i) Random alignment before, ii) photopolymerization during, and iii) scanning alignment after SWaP. Reproduced with permission.[31] Copyright 2017, American Association for the Advancement of Science. f) SLM-based dynamic mask photopatterning system. L1, L2, L3: lenses, QWP1, QWP2: quarter-wave plates, P1, P2: polarizers, where P2 is used to visualize the polarization patterns and will be removed during the exposure process. Reproduced with permission.[29] Copyright 2016, Optical Society of America.

1903665 (5 of 21)

ADVANCED
SCIENCE NEWS
www.advancedsciencenews.com

ADVANCED
MATERIALS
www.advmat.de

specific LC GPOEs. However, their quality and resolution are limited by the LC polymer masks.

Mask-free or dynamic-mask exposure systems have been exploited to improve the controllability and flexibility of the photoalignment technology. As a straightforward strategy, Miskiewicz and co-workers demonstrated the direct-writing approach as illustrated in Figure 4c.[10,57] The polarization direction of exposure light is dynamically controlled by an active polarization modulator. A 2D positioning stage is adopted for continuous scanning of the focused laser beam to write the designed geometric structures. A high resolution up to 1 μm can be achieved. However, a very long exposure time, such as ≈1 h,[58] is inevitable using this point-by-point process, especially for large-area patterning. To make the fabrication more time-efficient, Culbreath et al. and Wu et al. introduced the digital micromirror device (DMD)-based microlithography system.[28,44,59] As schematically depicted in Figure 4d, a collimated light beam is reflected onto the DMD, which serves as a dynamic mask. The DMD consists of numerous pixelated micromirrors, and each mirror can be independently switched between "on" and "off" states according to the loaded images. The patterned light reflected by the "on" state mirrors will be projected onto the LC cells through an objective lens and a motorized rotating polarizer. A CCD is utilized to monitor the focusing process. Based on this DMD system, Chen et al. proposed a multistep, partially overlapping exposure technique[60] for the continuous LC orientations in GPOEs. Recently, Hisano et al. developed a dye-free photoalignment technique based on the concept of scanning wave photopolymerization.[31,61] As shown in the inset of Figure 4d, with scanning of the focused guided light, a mass flow is triggered in the LC polymer film or chemical systems as the polymerization reaction propagates, leading to the patterned alignment of LCs with their slow axes along the scanning direction. Combined with the DMD system, arbitrary complex LC geometric patterns, e.g., the words "Tokyo Tech," can be achieved through such a photopolymerization process. In addition, Kobashi et al. used an LCD-type projector as a dynamic mask to implement the multistep exposure.[32]

Comparatively speaking, the single-exposure strategy has the greatest advantage considering time consumption and operation convenience. An effective method is based on interference or holographic lithography. When an object wave with a particular phase profile and a coherent reference wave are superimposed, the former will be recorded into the amplitude of the interference pattern. In particular, a spatially linear polarization distribution of the interference wave can be achieved when the object and reference waves are orthogonally circularly polarized. A Mach–Zehnder type interferometer is revealed in Figure 4e.[10] A laser beam is divided into the object (O) and reference (R) arms with orthogonal linear polarizations by a polarizing beam splitter (PBS). The object beam will carry the desired phase profile after passing through the object and then be recombined with the reference beam by another PBS. A QWP is set to transform these two beams into orthogonal circular polarizations. The setup can enable the recording of nearly any object's wavefront as an LC GPOE. As a more direct route, De Sio et al. achieved single-exposure photopatterning with the assistance of an SLM (Figure 4f).[29] The system consists of a pair of lenses to expand and collimate the laser beam,

a polarizer, and a QWP placed in sequence to ensure the circularly polarized illumination on the SLM. The SLM is an LC-based birefringent element composed of a pixel array with 256 gray levels that can be separately driven via external voltages. Different gray levels from pixel to pixel correspond to different phase retardation modulations of the incident beam. The spatially variant linear polarization distribution is further obtained after the beam passes through another QWP with an axis set at −45° with respect to the direction of the first polarizer. The lens functions to image the patterned light onto the LC cell or substrate coated with photoalignment material. Li et al. simplified this system with only one QWP in addition to the lenses and polarizer.[62] Moreover, the dynamic phase mask on the SLM can be conveniently reconfigured, inspiring on-demand and instant LC GPOEs.

4. Nematic LC-Mediated Geometric Phase

Using the photopatterning systems introduced above, varieties of LC GPOEs have been demonstrated to effectively modulate the geometric phase, from the traditional phase such as the linear or parabolic profile, to the novel structured one such as the spiral or cubic phase. As a well-established and affordable technology, LCs in the nematic mesophase offer interesting material properties, especially broadband and large optical birefringence, good electro-optical tunability, high stability, commercial availability, and roughly no absorption in the visible band. Therefore, nematic LCs have been thoroughly exploited in the demonstration of versatile GPOEs. In this section, typical transmissive geometric-phase planar optics based on nematic LCs are briefly discussed.

4.1. Traditional Phase Modulation

Traditional optical elements have long been used for modulation of the amplitude, phase, and polarization of light. Among numerous modulators, gratings and lenses, which can be regarded as linear and parabolic phase modulation, respectively, have been widely studied due to their crucial applications in beam steering, optical communications, spectroscopy in chemistry and astrophysics, virtual reality (VR), augmented reality (AR), and 3D displays. With the combination of nematic LCs and the geometric phase, transmissive LC polarization gratings (PGs) and geometric phase lenses (GPLs) are first created with good electro-optical tunability, polarization selectivity, and nearly 100% diffraction efficiency.

The LC PG features periodic linearly varying directors (**Figure 5**a), the local optical axis orientation in the x–y plane of which can be generally expressed as $\alpha_{PG} = \frac{-\pi x}{\Lambda}$ (Λ is the period of PG).[63] Referring to the Jones matrix calculation in Section 2, it can be observed that the PG has only three diffraction orders: the 0th order with the same polarization as incident light and the ±1st orders with orthogonal circular polarizations. Under the half-wave condition, only ±1st orders remain with the 0th order eliminated. Moreover, for the circularly polarized incidence, there is only one first order with a converted
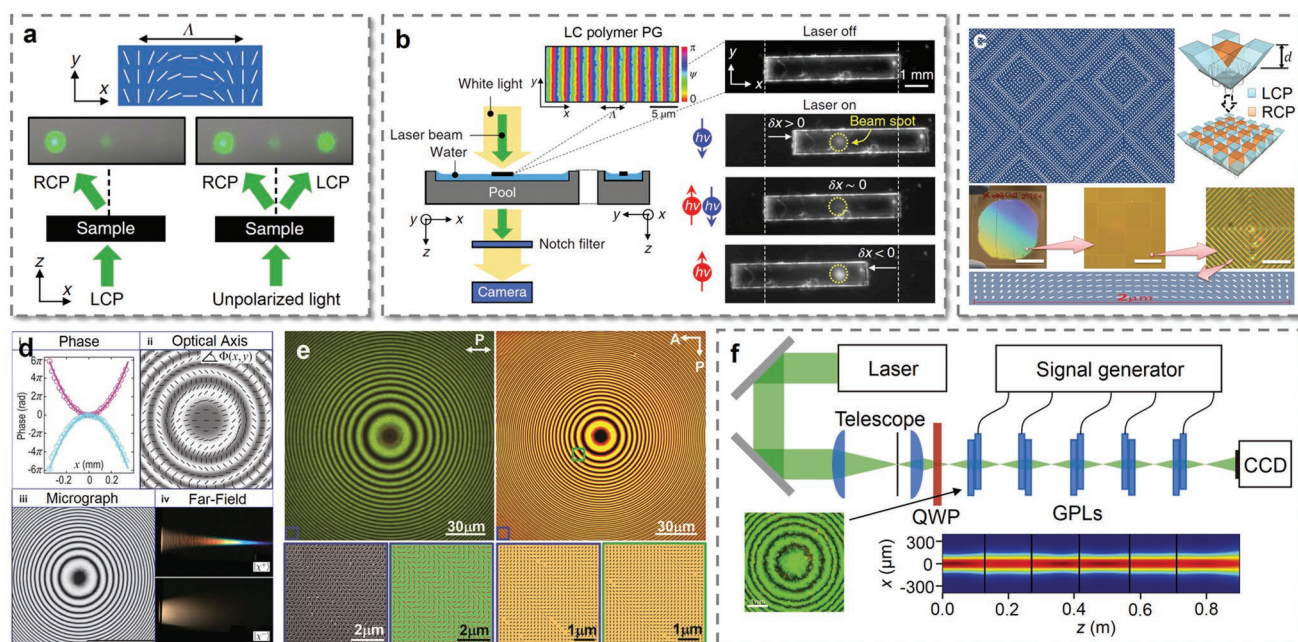
Figure 5. Nematic LC-mediated PGs and GPLs. a) The spatially variant director distribution, diffraction behaviors with LCP, and unpolarized incident light of the LC PG. Reproduced with permission.[72] Copyright 2018, Nature Publishing Group. b) Setup for the macroscopic observation of the spin-dependent optical force based on the LC polymer PG slab, and displacements observed under the illumination of spin up and spin down photons. Reproduced with permission.[72] Copyright 2018, Nature Publishing Group. c) Schematic diagrams of the alignment structure and director distribution for construction of the holographic polarizer and light propagation through the LC polymer PG domains. Photograph and micrographs of the LC polymer film, with the white scale bar indicating 10 mm, 150 μm, and 5 μm, respectively. Reproduced with permission.[73b] Copyright 2015, Wiley-VCH. d) Primary (magenta) and conjugate (cyan) phases, optical axis, micrograph, and far-field diffraction results of LC GPL. Reproduced with permission.[10] Copyright 2015, Optical Society of America. e) Micrographs of the PMM and the LC polymer micro-GPL with f-number $N_f = 2$. SEM image and measured polarization directions of the light transmitted through the blue square area in the micrograph of PMM; molecular orientations in the blue and green square areas in the micrograph of LC GPL. Reproduced with permission.[55] Copyright 2019, Wiley-VCH. f) Optical setup for guiding light based on five LC GPLs and the guided mode obtained for the RCP incident. Reproduced with permission.[89] Copyright 2016, Nature Publishing Group.

circular polarization state. Theoretically, a 100% diffraction efficiency can be achieved. Cipparrone et al. and Ono et al. were among the first researchers to fabricate PGs via a holographic recording method in polymer dispersed[64] or photocrosslinkable polymer[65] LC systems. The cis–trans isomerization photosensitive materials were further adopted as the alignment layer to successfully improve the diffraction performance.[27,66,67] Fine structures with spatial periodicities of 5–8 μm,[27] and even 2.1 μm,[67] were obtained, leading to a high efficiency of up to 98%. For the commonly used nematic LCs, the response time is on the millisecond scale. By introducing the dual-frequency LC into the PG, Duan et al. proposed a fast-response optical switch, for which the switching time reached as low as the sub-millisecond.[68] Recently, Guo et al. reported much faster beam steering within tens of microseconds by means of an extra ferroelectric LC phase shutter.[69] Additionally, 2D and even 3D PGs were demonstrated through multibeam interference,[70] with an interesting verification of the polarization selectivity presented via a beetle *Plusiotis gloriosa*.[71]

For conventional LC PGs, a very unique application is the macroscopic observation of spin-dependent lateral forces and unusual left-handed torques (Figure 5b), as verified by Magallanes and Brasselet.[72] The experiments were conducted using the 1D LC polymer PG layer and disk-shaped rotors composed of four-quadrant PGs with clockwise or anticlockwise

orientational gradients, respectively. The resultant forces were on the order of 1 nN and led to 0.5 mm displacements in less than 100 s. By integrating patterned LC PGs and wave plates, Du et al. proposed the holographic thin-film polarizer.[73] As presented in Figure 5c, each unit of the polarizer is composed of four LC polymer PG domains with all grating vectors pointing to common centers. With the assistance of a patterned LC polymer QWP, any unpolarized incident light will be converted to a linear polarization with the desired orientation. The experimental maximum extinction ratio of the holographic polarizer was ≈100:1, and the transmittance was as high as 91%. Additionally, LC PGs have also been widely applied in the detection of light polarization state,[74] polarization insensitive imaging,[75] achromatic beam splitting,[76] controlling of colloidal placement,[77] and VR/AR displays.[78]

Regarding information displays, another important kind of LC GPOE is the GPL, with an optical axis distribution following $\alpha_L = \dfrac{\pi\left(\sqrt{r^2 + f^2} - f\right)}{\lambda}$, where r and f are the radius ($r^2 = x^2 + y^2$) and the designed focal length, respectively. In general, $r \ll f$, and thus, the LC director distribution of the GPL can be simplified as $\alpha_L = \pi r^2/2f\lambda$, indicating a parabolic modulation of the phasefront. Under the half-wave condition, the output light passing through the GPL carries a phase factor of $\exp(\pm i\pi r^2/f\lambda)\chi^{(\mp)}$.

**ADVANCED
SCIENCE NEWS**

www.advancedsciencenews.com

**ADVANCED
MATERIALS**

www.advmat.de

Therefore, it functions as a converging lens with focal length f for the RCP incident beam despite a diverging lens for LCP, revealing a helicity-dependent focusing/defocusing property (Figure 5d). LC GPLs have been attracting increasing attention due to their promising applications in head-mounted 3D display for AR/VR.[48,79] Additionally, it is worth mentioning that their combination with conventional refractive lenses can reduce the chromatic aberration of the whole display system.[48]

To date, the fabrication of LC GPLs and corresponding microlens arrays has occurred mainly via holography photopatterning methods.[10,80] Nanoimprinted alignment[81] and two-photon polymerization direct-laser writing[82] techniques can also be introduced. Very recently, Jiang et al. created a remarkable LC GPL based on the PMM-mediated photopatterning system (Figure 5e).[55] A low f-number of 2 with the smallest pitch of 1.5 μm for the periodic LC molecular orientation was achieved. Colloidal particles with a diameter of 5 μm were clearly observed through such low f-number LC GPL-based imaging systems, revealing the diffraction-limited quality. Additional efforts have been devoted to the design of lens structures, LC materials, and optical systems. Tabiryan et al. achieved focal length switching by stacking two LC GPLs.[83] By further utilizing two and four LC polymer layers of opposite chirality, Tabiryan et al. demonstrated broadband GPLs encompassing the visible band from 450 nm to more than 700 nm and the near-infrared band from 650 nm to more than 1000 nm, respectively.[84] Zhan et al. designed the polarization-independent GPL system by combining several LC GPLs together with specific intervening distances.[85] Zhou et al. produced a kind of integrated GPL by sequentially placing the LC polymer PG and GPL as photomasks, achieving the spatial separation of the focusing and defocusing order.[86] To improve the switching time, Ma et al. and Duan et al. introduced fast-response ferroelectric[87] and dual-frequency[88] LCs into the continuous alignment of the lens structure, respectively. In a very impressive work, Slussarenko et al. presented the transverse confinement of electromagnetic waves using a series of discrete LC GPLs, achieving the guidance of light beyond the Rayleigh length (Figure 5f).[89] Afterward, Jisha et al. demonstrated the self-trapping of light by creating its own geometric phase waveguide due to the optical nonlinearity.[90]

4.2. Spiral Phase Modulation

The past few years have witnessed sustained extensive attention and impressive progress in extraordinary phase modulation toward spatially structured light. The typical example, the optical vortex (OV) associated with spiral phase control, has remained a hot topic of intense scientific curiosity in both classical and quantum optics.[91] It features a helical phase-front $\exp(im\phi)$, where ϕ is the polar coordinate and m is the topological charge representing the quantization of the induced orbital angular momentum (OAM) of light.[92] The phase singularity at the axis causes a zero intensity region in the center, leading to the donut-shaped intensity distribution (**Figure 6**a). These distinguished properties endow OVs with a wide range of applications including optical tweezers,[93] stimulated emission depletion microscopy,[94] optical communications,[95] quantum

informatics,[96] and the observation of extrasolar planets.[97] To implement spiral-phase modulation via the geometric phase, a special LC GPOE with an optical axis distribution obeying $\alpha_q = q\phi + \alpha_0$ can be introduced. This represents the well-known expression of the so-called "q-plate,"[9,98] where $q = m/2$ and α_0 is the constant. For a circularly polarized light passing through the q-plate under half-wave condition, the emerging wave will be transformed into the spiral phase $\exp(\pm i2q\phi)$ with an incident polarization-dependent sign (Figure 6d). Additionally, the circular polarization state of the generated OV is orthogonal to the input, indicating coupling between the spin and OAM. Notably, as shown in Figure 6e, changing the incident light to linear polarization will result in another donut-shaped light field, i.e., the vector beam.[99] The vector beam is characterized by spatially variant polarization states and plays an important role in high-resolution imaging, optical trapping, laser processing, and optical communication.[100]

In 2006, Marrucci et al. first proposed this famous LC GPOE and demonstrated it via the circular-rubbing method.[9,42,101] Given the invention of the photoalignment technology, LC q-plates with higher orders and more complicated structures have been successively achieved. By adopting the rotating photopatterning system combined with the SD1 as the alignment material, Slussarenko et al. produced q-plates with different charges (Figure 6b).[50] Fan et al. also acquired vector beams for circularly polarized inputs using a specific q-plate under the quarter-wave condition.[51] Through the DMD-based dynamic exposure technique, Ji et al. proposed the concept of the meta-q-plate with a q and α_0 that could be arbitrarily altered (Figure 6c).[102] Additionally, by integrating PGs with q-plates, forked polarization gratings were proposed to spatially separate the LCP and RCP OV orders with opposite topological charges.[60,103] Tam et al. reported a vortex lens featuring the integrated geometric phase of the lens and q-plate, enabling the focusing or defocusing of orthogonal OVs.[56] With further superposition of all three profiles, Duan et al. designed a forked vortex lens, achieving the generation and separation of focused and defocused OVs simultaneously.[104] Moreover, Chen et al. designed the Dammann-q-plate[105] by introducing the 2D Dammann grating structure[38,106,107] to digitalize the spiral geometric phase of the q-plate (Figure 6f). An equal-energy array of the OV or vector beam, i.e., higher-order Poincaré sphere beam lattices, was generated. Subsequently, the combination with circular Dammann grating induced the perfect high-order Poincaré sphere.[108] Vector vortex beams have also been reported by stacking q-plates with QWPs or electrically tunable LC wave-plates.[109] Nematic LC material with a large birefringence has been employed to extend the use of the q-plate to manipulate the terahertz vortex wave.[110]

Additionally, spiral geometric phase modulation can also be achieved through the intrinsic topological defects existing in nematic LCs.[111] By dispersing the nematic 5CB in water and adding cetyl-trimethyl-ammonium bromide surfactant, Brasselet et al. obtained droplets with a diameter of a few micrometers and a spherically symmetric 3D spatial distribution (Figure 6g).[112] When the droplets are trapped by circularly polarized Gaussian beams, the on-axis radial birefringence distribution will give access to the conversion of OVs. On the other hand, the umbilic is a kind of defect that naturally presents a vortex-like morphology. Such defects usually occur in nematic
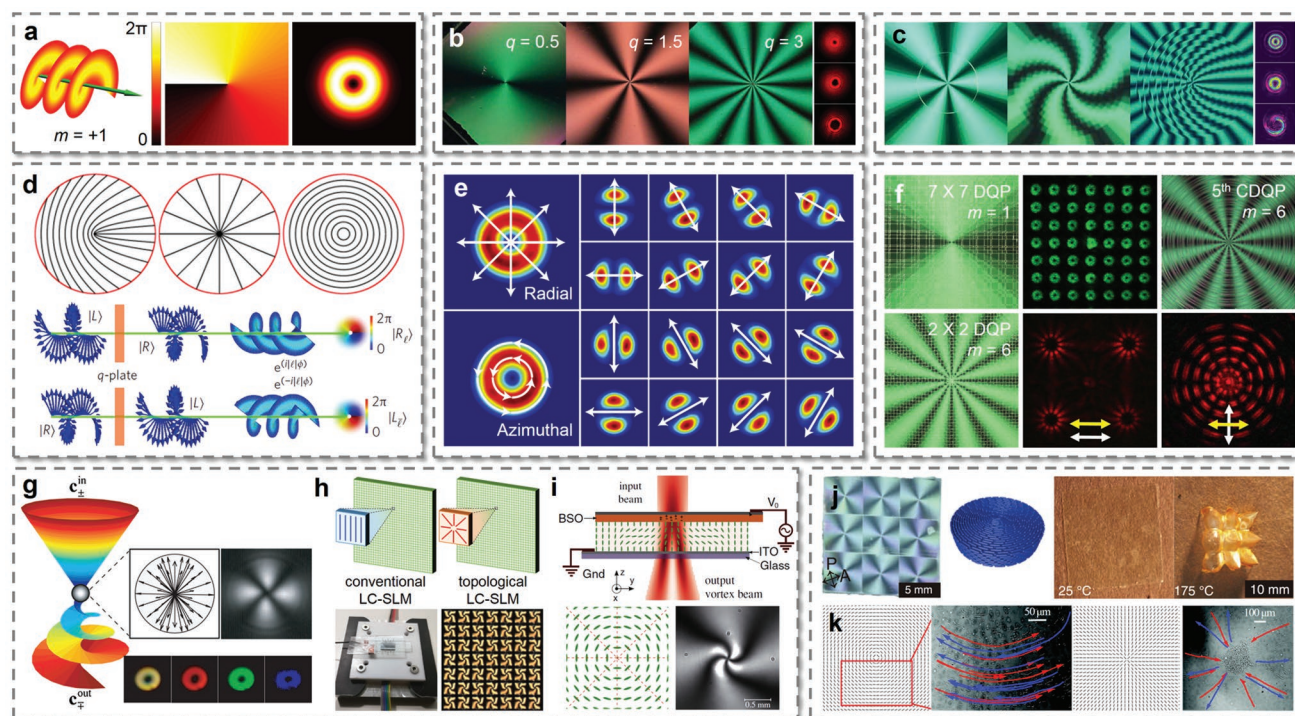
Figure 6. OV induction via nematic LCs. a) Schematic illustration of the helical wavefront, transverse phase distribution, and intensity distribution of the OV with $m = +1$. b) Micrographs of the q-plates with $q = 1/2$, $q = 3/2$, and $q = 3$, fabricated via the rotating photopatterning system, and the corresponding generated OVs. Reproduced with permission.[50] Copyright 2011, Optical Society of America. c) Micrographs of the meta-q-plates with $q = 1.5$, α_0: 0 at $r \leq 0.5r_0$, $\pi/2$ at $r > 0.5r_0$; $q = 1.5$, α_0: from 0 at the center increases to $\pi/2$ at $r \geq 0.9r_0$ with an interval of $\pi/18$ every $0.1r_0$; $\alpha_0 = 0$, q: from 2 at $r \leq 0.1r_0$ increases to 6.5 at $r > 0.9r_0$ with an interval of 0.5 every $0.1r_0$, fabricated via the DMD-based dynamic photopatterning system and corresponding generated complex OVs. Reproduced with permission.[102a] Copyright 2016, Nature Publishing Group. d) Geometries of q-plates with $q = 1/2$, $\alpha_0 = 0$; $q = 1$, $\alpha_0 = 0$; $q = 1$, $\alpha_0 = \pi/2$, and illustration of the optical function of the q-plate on the circularly polarized plane wave: the output is a helically phased beam with an orthogonal circular polarization. Upper row reproduced with permission.[9] Copyright 2006, American Physical Society. Bottom row reproduced with permission.[99b] Copyright 2016, Nature Publishing Group. e) Radially and azimuthally polarized vector beams generated under the illumination of horizontally and vertically linear polarizations on the q-plate with $q = 1/2$, $\alpha_0 = 0$, and corresponding lobe structures when analyzed by a linear polarizer with directions indicated by double-ended white arrows. Reproduced with permission.[99b] Copyright 2016, Nature Publishing Group. f) Micrographs of the 7×7, 2×2 Dammann-q-plates with $m = 1$, $m = 6$ and the fifth order circular-Dammann-q-plate with $m = 6$, and respectively generated (perfect) higher-order Poincaré sphere beam lattices. First two columns reproduced with permission.[105] Copyright 2017, American Chemical Society. Third column reproduced with permission.[108] Copyright 2018, American Physical Society. g) Illustration of OV generation from a nematic LC droplet. Insets: schematic radial structure, micrograph of the LC droplet, the generated polychromatic OV, and its RGB components. Reproduced with permission.[112] Copyright 2009, American Physical Society. h) Illustration of a conventional LC SLM with uniform pixels and the proposed topological LC SLM with structured pixels. Fabricated LC SLM based on LC topological defects and micrograph of a matrix of 49 q-plates with $|q| = 1$. Reproduced with permission.[114] Copyright 2018, American Physical Society. i) Schematic of the LC light valve, sketch of the LC director in the x–y plane, and the intensity profile observed with crossed polarizers under white light illumination. Reproduced with permission.[118a] Copyright 2012, American Physical Society. j) Micrograph, director orientation, and photographs of the voxelated LC elastomer film based on the q-plate structure. Nine cones arise upon heating and reversibly flatten upon cooling. Reproduced with permission.[58] Copyright 2015, American Association for the Advancement of Science. k) Circular and radial movements of the bacteria in the lyotropic chromonic LC q-plates with $q = 1$, $\alpha_0 = \pi/2$ and $q = 1$, $\alpha_0 = 0$, respectively. Reproduced with permission.[43] Copyright 2016, American Association for the Advancement of Science.

LCs with negative dielectric anisotropy and a perpendicular alignment when the applied voltage exceeds the Fréedericksz transition threshold.[113] Nassiri and Brasselet utilized these umbilical defects to fabricate a programmable LC SLM, enabling the multispectral generation and modulation of the OV array (Figure 6h).[114] Salamon et al. employed the topological dislocation of lattice defects to generate tunable OV arrays with different topological charges.[115] In addition, with the combination of a static magnetic field from an annular magnet, Brasselet achieved a macroscopic q-plate with a centimeter size.[116] These microstructures induced by droplets or umbilical defects are basically limited to $q = 1$ or $q = 1/2$. By taking advantage of

the Schlieren texture, which can result from doping the 5CB with the nonmesogenic molecular compound leucoquinizarin, Loussert et al. created a $q = 3/2$ topological defect, extending the OAM range of the generated OVs.[117]

Barboza et al. introduced the photoconductor material $Bi_{12}SiO_{20}$ (BSO) to create an optically induced q-plate structure and corresponding lattices.[118] As shown in Figure 6i, the LC cell is composed of negative nematic LC sandwiched by a glass plate and a slab of the transparent BSO, the interior surfaces of which are treated for homeotropic LC anchoring. When a circular polarized Gaussian beam is incident on the BSO slab, the photogenerated charges increase the voltage applied to the

**ADVANCED
SCIENCE NEWS**

www.advancedsciencenews.com

**ADVANCED
MATERIALS**

www.advmat.de

covered LC region. Accordingly, the LC director is reoriented following the intensity gradients associated with the Gaussian beam profile and the rotational structure of the electric field lines, leading to spontaneous induction of the topological defect in the nematic LC texture. Aleksanyan et al. used such a LC light valve as a vortex coronagraph to directly observe faint companions close to multiple-star systems.[119] It is worth mentioning that, in addition to the common OV generation, the topological defects in q-plate structures can also be applied in the construction of LC elastomer actuators (Figure 6j)[58,120] and the command of colloidal objects[52] or active matters (Figure 6k).[43] In brief, q-plate-based LC microstructures have not only provided a versatile platform for spin-to-OAM conversion, but also enriched the area of light structuring and fruitful applications.

4.3. Other Structured Phase Modulation

Further exploiting advanced geometric phase modulation will give rise to numerous light beams with a customized intensity, polarization, and phase. During the last dozen years, enormous interests have been focused on Airy beams, which possess intriguing nondiffraction, transverse acceleration, and self-healing properties.[121] These special features have promoted a variety of applications such as nanoparticle manipulation, curved plasma channel, spatiotemporal light bullets, light-sheet microscopy, and material processing.[121] The acquisition of Airy beams occurs mainly through the cubic phase modulation of the Gaussian beam followed by a lens to perform the Fourier transformation.[122] Hence, the optical axis of the corresponding GPOE to generate Airy beams should obey $\alpha_A = \frac{x^3 + y^3}{2}$.[123,124] When a circularly polarized light illuminates it under the half-wave condition, the output field will be modulated into $\mathbf{E}_{out} = \exp[\pm i(x^3 + y^3)]\chi^{(\mp)}$. The sign of the induced cubic phase item is also associated with the handedness of the circular polarization, and "$\pm$" indicates that the RCP and LCP Airy beams accelerate along opposite directions. Through the SD1- and DMD-based dynamic photopatterning technique, Wei et al. carried out the above design as the LC polarization Airy mask, achieving the generation of single and dual Airy beams with polarization-controllable characteristics (**Figure 7**a).[124] For dual Airy beams, the distance between two main lobes directly reflects the transverse deflection, which provides a more convenient and accurate way to characterize the self-accelerating property. Afterward, via the combination of the LC q-plates, vortex Airy beams were proposed, and the transverse accelerating, self-healing, and quasi-nondiffracting OVs were verified.[125] Through further integrating the director distributions of the q-plate and Airy mask, LC q-Airy-plates were invented, supplying a more compact configuration for the generation of vortex Airy beams with a higher efficiency of greater than 90% (Figure 7b).[126]

Other structured beams with featured phase-front (Φ) can also be expected through the LC GPOEs by setting the LC director orientations as $\alpha = \Phi/2$. For example, Ruiz et al. reported the generation of nondiffracting Bessel and Weber beams by polarization holography (Figure 7c).[127] The holograms were recorded in polarization-sensitive films by the interference between a reference plane wave and a tailored

complex beam with orthogonal circular polarizations. Similarly, based on the DMD dynamic exposure system, Larocque et al. fabricated a LC GPOE with an optical axis satisfying $\alpha = (k_\rho \rho + m\phi)/2$.[128] The resultant optical field is thus proportional to $J_m(k_\rho \rho)\exp(m\phi)$, where k_ρ is the radial component of the wave-vector and J_m is the mth order Bessel function of the first kind, that is, the nondiffracting Bessel beam. As shown in Figure 7d, helical Ince–Gauss beams were also generated in a similar way. The even and odd mode of the generated Ince–Gauss beam could be recovered by analyzing the output linear polarization component. Beyond the high-efficiency and polarization-sensitive generation of various structured light, nematic LC GPOEs can be further employed in their manipulation and detection, such as the recently reported shearing interferometry[129] and topical OAM sorting (Figure 7e).[130] Generally, it is a powerful tool for light control, inspiring numerous novel optical devices and practical applications.

5. Chiral LC Superstructure-Mediated Geometric Phase

Previously discussed nematic LC-mediated transmissive GPOEs, which can be considered as a special wave-plate with space-variant optical axes, usually suffer from intense wavelength-dependent efficiency. According to Equation (4), the half-wave condition should be precisely satisfied to maximize the conversion efficiency. Although the electro-optical tunability of nematic LCs could make the same device available for different respective wavelengths, the broadband high efficiency is still challenging, restricting their applications in many fields with wavelength independence requirements.

5.1. Reflective Geometric Phase from Chiral LC Superstructures

Nature always solves complicated problems in simple manners, inspiring scientists to find solutions by mimicking natural structures. Chiral superstructures are ubiquitous wonders found in nature, from galaxies, beetle exoskeletons, bindweed plants, to DNA.[131] Some representative examples are presented in **Figure 8**a–c. They trigger curiosities toward insights of intriguing natural materials and inspire novel artificial architectures.[132] Given the intrinsic rapid and cost-effective formation, self-assembled soft matter is a promising building block for constructing such chiral superstructures. Among them, CLC is fascinating, with a wide range of feature sizes and extrastimuli tunability.[35–37] CLC is a topical chiral liquid crystalline phase, where the orientations of rod-like molecules are slightly twisted with respect to their neighbors and overall self-assemble into a periodic helical superstructure.[16] As shown in Figure 8d,e, the molecular long axes and hence the directors are always perpendicular to the helical axis of the CLC chiral superstructure, which can be either left-handed or right-handed. Depending on the helical pitch and surface boundary conditions, CLCs normally exhibit three distinctive textures: Grandjean texture (also known as a planar texture or standing helix state), fingerprint texture, and focal conic texture.[133] In the planar texture, the helical axis is perpendicular to the substrate, while it lies in
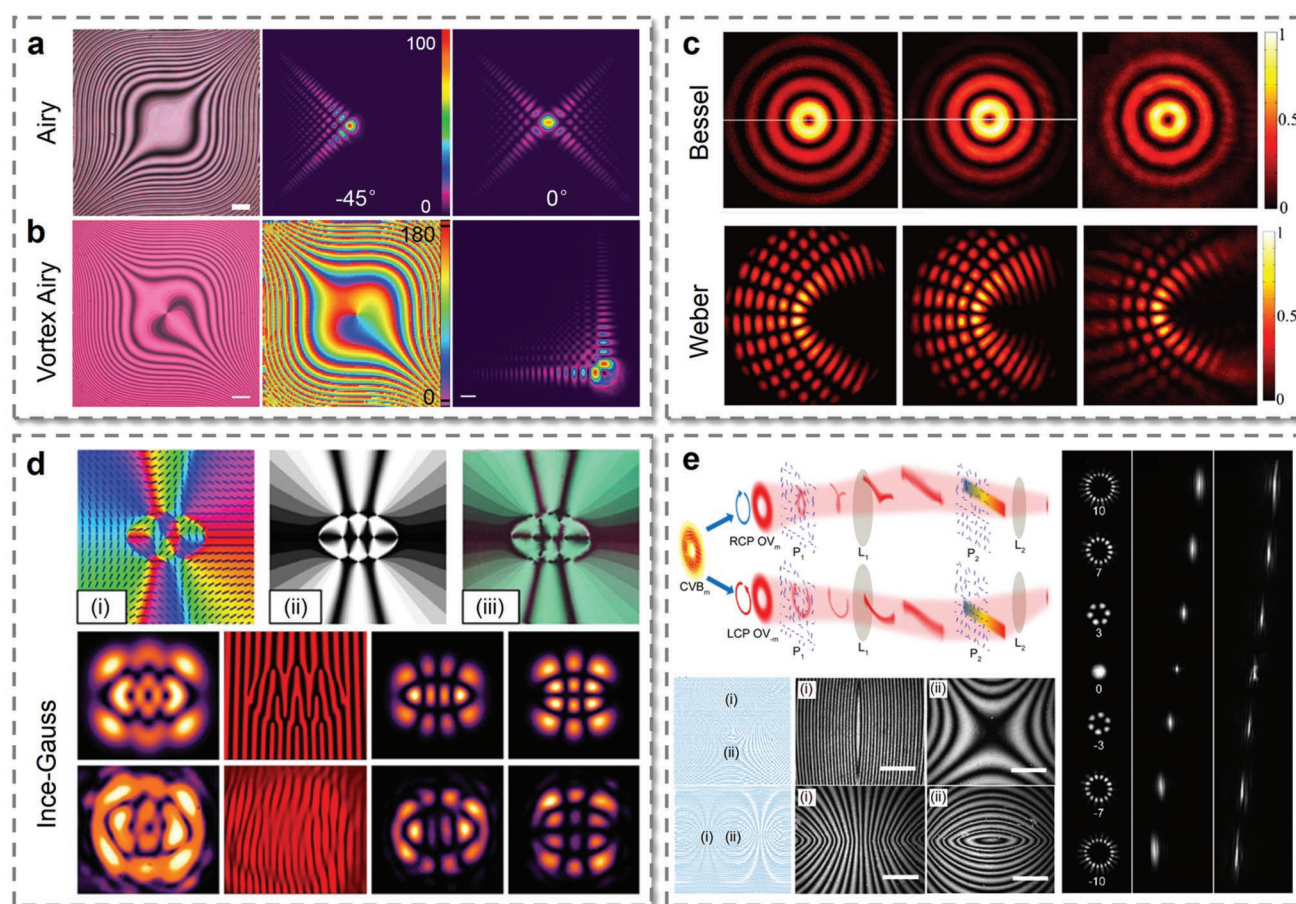
Figure 7. Advanced beam structuring by nematic LC GPOEs. a) Micrograph of the LC polarization Airy mask and generated polarization-controllable Airy beams with RCP (−45°) and linearly polarized (0°) incidence. Reproduced with permission.[124] Copyright 2015, Nature Publishing Group. b) Micrograph, measured director distribution of the LC q-Airy-plate with $q = 0.5$, and the generated vortex Airy beam. Reproduced with permission.[126] Copyright 2018, American Institute of Physics. c) Intensity distributions of the first order Bessel beam and the third order odd Weber beam generated by the SLM, the liquid crystalline azo-polymer-based GPOEs, and respective later ones propagating in the plane $z = 30$ cm. Reproduced with permission.[127] Copyright 2013, Optical Society of America. d) Optical axis distribution, expected and experimental micrographs of LC GPOE to generate an Ince–Gauss beam. Simulated and experimental results of the interference, even mode and odd mode patterns of the generated Ince–Gauss beams. Reproduced with permission.[128] Copyright 2016, IOP Publishing. e) Schematic of OAM sorting based on the spin-dependent optical geometric transformation enabled by LC GPOEs. The color map from red to blue indicates the phase gradient. P1, the geometric transformation device; P2, the phase correction device; L1, L2, optical lenses. Fast-axis orientation distributions and local micrographs of these two LC GPOEs. Measured intensity distributions of the incident vector beams of the order 10, 7, 3, 0, −3, −7, and −10 after the linear polarizer, calculated sorting results with displacements proportional to their orders, and corresponding experimental results. Reproduced with permission.[130e] Copyright 2018, American Chemical Society.

plane in the fingerprint texture. For the focal conic texture, the helical axis is randomly oriented.

Considering the planar texture, periodic modulation of the optical anisotropy of the LC material results in a helical-variant dielectric tensor, leading to a natural 1D photonic crystal featuring a photonic band gap.[134] For light propagating along the helical axis, a broadband Bragg reflection with unique circular-polarization (spin) selectivity is exhibited over a wavelength range of $\Delta\lambda = n_o p - n_e p$, where p is the helical pitch, and n_o/n_e are the ordinary/extraordinary refractive indices, respectively.[17] The circularly polarized light with the same handedness as the chiral helix of CLCs is completely reflected, while the other with the orthogonal circular polarization state is transmitted. The theoretical transmittance spectrum of a planar CLC at the normal incidence with an unpolarized light and corresponding micrograph are shown in Figure 8f,g, respectively. Given the

unique optical performance together with the intrinsic versatile stimuli-responsive characteristics, CLCs have long been a booming topic in material science and are actively being pursued in wide application fields,[135] including reflective displays,[136] switchable polarizers and color filters,[137] non-mechanical beam steering,[138,139] manipulation of nanoparticles,[140] and mirrorless tunable lasers.[141,142]

In 2016, the spin–orbit geometric phase was discovered for the light reflected off planar CLC superstructures,[32–34] and immediately attracted extensive attention, becoming one of the most emerging frontiers for soft matter and planar optics. Such a distinctive reflective geometric phase in CLCs is attributed to the preservation of the polarization helicity from circular Bragg reflection.[33] In contrast to the reversion of circular polarization reflected on a common mirror, the circularly polarized light maintains its polarization state after reflecting from a CLC,
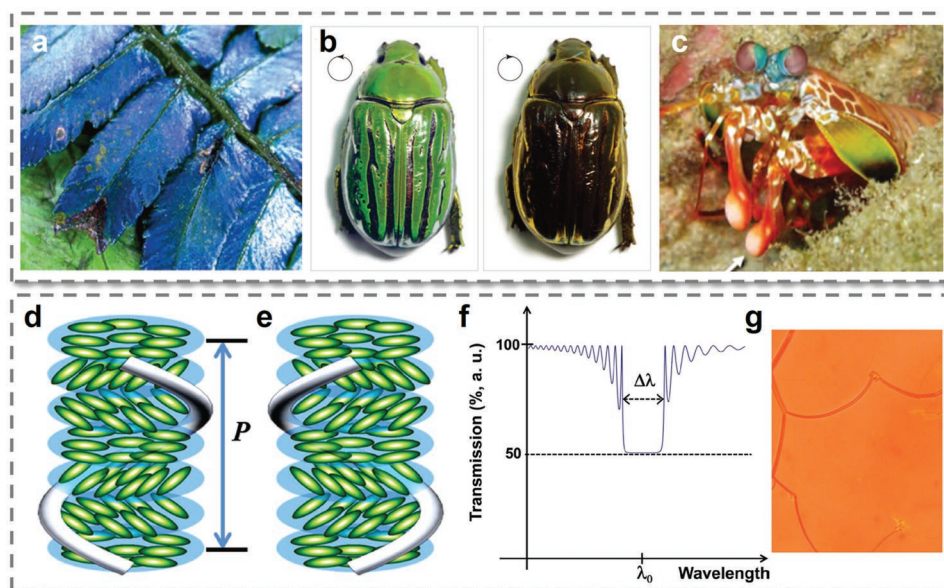
Figure 8. Natural wonders of CLC-like organization in plants and animals. a) Photograph of the leaves of *Diplazium tomentosum*. Reproduced with permission.[131c] Copyright 2014, Elsevier. b) Photographs of the beetle *Chrysina gloriosa*. Left: the bright green color seen in unpolarized light or with a left circular polarizer; right: the green color is mostly lost when seen with a right circular polarizer. Reproduced with permission.[131a] Copyright 2009, American Association for the Advancement of Science. c) Photograph of a stomatopod species *Odontodactylus scyllarus*. Reproduced with permission.[131b] Copyright 2012, American Association for the Advancement of Science. Molecular organizations in d) left-handed and e) right-handed CLCs. Reproduced with permission.[37a] Copyright 2018, Wiley-VCH. f) Theoretical transmittance spectrum of a planar CLC at the normal incidence with an unpolarized light. Reproduced with permission.[132] Copyright 2012, Wiley-VCH. g) The planar or Grandjean texture of CLCs under a polarized optical microscope, where oily streak defects usually appear. Reproduced with permission.[141] Copyright 2010, Nature Publishing Group.

while the propagation direction becomes opposite, which indicates flipping the optical spin angular momentum. The SOI effect of light will occur in this progress, and accordingly, a phase factor independent of the optical path will be introduced into the reflected light, i.e., the reflective geometric phase. For an inhomogeneously aligned planar CLC, the magnitude of such a phase change is proportional to the initial orientation angle of the local director at the substrate surface, which can sometimes be called "the helix phase" for short.[32,143] The CLC-mediated reflective geometric phase also exhibits a handedness-dependent sign, conjugated for opposite chirality of CLC superstructures.

Figure 9a–d shows the optical properties of a right-handed CLC based on Berreman's 4×4 matrix method simulated by Kobashi et al.[32] When RCP light is normally incident, Bragg reflection occurs between 600–680 nm, and the reflected phase varies with the wavelength (Figure 9a). The reflected phase can also be changed synchronously with the varied helix phase for a single wavelength, while the reflectivity is maintained (Figure 9b). The acquired geometric phase is twice the value of the helix phase; that is, a π variation in the helix changes the reflected phase by 2π. Given the head–tail symmetry of the uniaxial LC director, full phase control over $0-2\pi$ can be rationally expected. Moreover, Figure 9c,d verifies that the transmitted LCP light experiences only a uniform dynamic phase change regardless of the helix phase, retaining the original phase-front. This result enables a spin-determined phase modulation with the perfect circular polarization selectivity. Owing to the spin-dependent Bragg reflection of CLC chiral superstructures, these devices can be tuned from fully reflective to totally transmissive

by altering the incident polarization. Additionally, such a novel class of GPOEs exhibits a uniform high efficiency over a broad band $(n_o p - n_e p)$, without any requirement for fine-tuning of the half-wave condition, in contrast to transmission nematic LC ones. Overall, it supplies a new platform for broadband reflective planar optics and may significantly upgrade existing optical apparatuses.

Via appropriately preprogramming and manipulating the spatial distribution of CLC standing helixes, a series of broadband planar photonic devices can be achieved with advanced functionalities. Because the formation of 3D CLC superstructures is driven by the intrinsic self-assembly capability, spatial control of the geometric phase is possible by defining the orientation at a certain position in space, which is easiest at the substrate surface.[32] Similar to those transmissive planar optics mediated by nematic LCs, photopatterning technology is usually employed for a point-to-point control of the director distribution on a substrate, and the self-organized CLC superstructures are guided by two parallel preprogrammed photoalignment films.

In initial research, Kobashi et al. proposed a reflective deflector featuring the periodically rotating CLC helical superstructure,[32,144] as shown in Figure 9e. It endows the reflected light with a linearly varying phase profile, as in the previously mentioned PG based on nematic LCs. Therefore, the CLC deflector is also referred to as polarization volume grating or Bragg PG.[145] It is characterized by visualizing the reflected phase with a Michelson-type microscopic interferometer and by observing the reflected spot of a normally incident He–Ne laser. For the RCP incidence, strong deflection occurs, while the
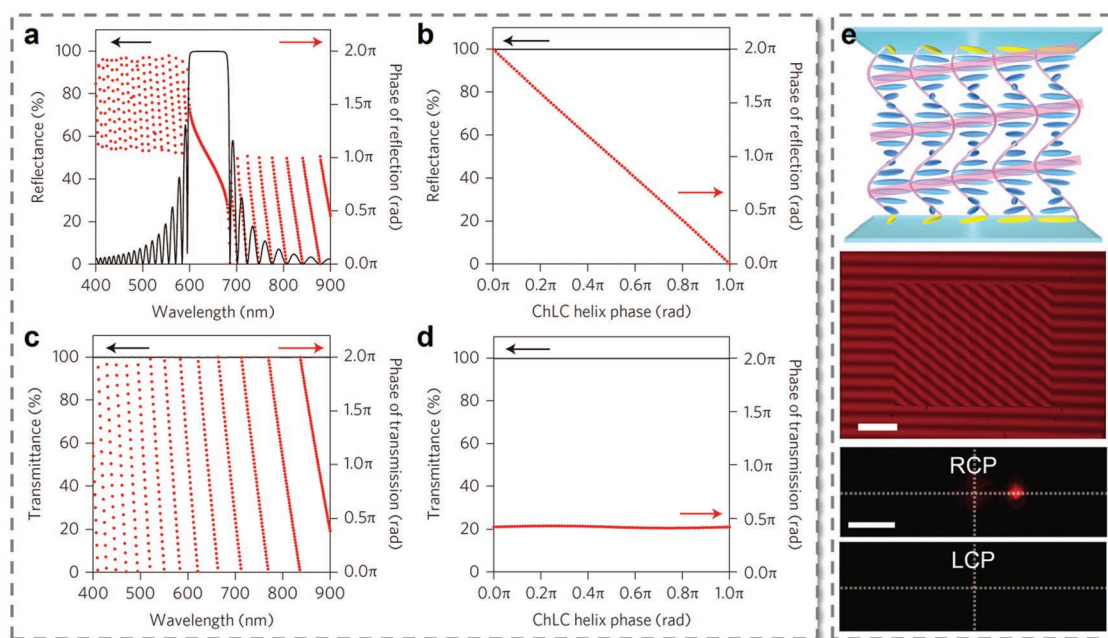
**ADVANCED
SCIENCE NEWS**

www.advancedsciencenews.com

**ADVANCED
MATERIALS**

www.advmat.de

Figure 9. Reflective geometric phase from CLCs. a) Simulated reflectance (black) and reflected phase (red) for RCP incidence on a uniformly aligned right-handed CLC with $n_e = 1.7$, $n_o = 1.5$, and $p = 400$ nm. b) Reflectance (black) and phase (red) for RCP light at the center wavelength of the Bragg band (640 nm), plotted as a function of the helix phase, which is defined as the orientation of the director at the substrate surface. c) Transmittance (black) and phase (red) for LCP incidence. d) Transmittance (black) and phase (red) for LCP light at 640 nm, plotted as a function of the helix phase. e) Reflective deflector with patterned CLCs. Top: schematic of the director distribution; middle: experimental interferograms obtained at ≈632 nm, scale bar: 200 μm; bottom: reflected laser spots from the sample with opposite circular polarizations, scale bar: 5 mm. Reproduced with permission.[32] Copyright 2016, Nature Publishing Group.

reflected spot almost vanishes on LCP incidence. The exhibited ultrahigh diffraction efficiency, unique polarization selectivity, high polarization contrast, and large diffraction angle make the CLC reflective deflector an attractive candidate for optical isolators and display areas. Wu's group has systematically studied the applications of this device in 2D/3D wearable displays, full-color waveguide displays, and AR displays.[145,146] Additionally, Kobashi et al. have also demonstrated a reflective CLC GPL.[32] The parabolic-variant alignment pattern induces a parabolic phase profile, which reverses the sign for the opposite viewing direction. Thus, the CLC GPL can either converge or diverge light depending on the incident side. A direct visualization of this difference was experimentally presented. The focusing state of the incidence can be switched simply by flipping the device. Recently, Serak et al. created an array of such a CLC lens and described new opportunities for polarizer-free displays, smart windows and other photonic technologies.[147]

5.2. Advanced Broadband Reflective Planar Optics

The flexible programming of these chiral superstructures through molecular surface pattern engineering enables on-demand beam structuring, and advanced broadband reflective planar optics can be further expected. As shown in **Figure 10**a, Mohri et al. introduced a random structure inspired by the *Morpho didius* butterfly into the distribution of CLC helixes.[148] Accordingly, the phase of reflected light becomes randomized, leading to a diffuse reflection that spreads over a wide angle

greater than ±30°. The diffuse reflection maintains its circular-polarization selectivity, making it unique compared with the butterfly itself or other artificial structures through mimicry of the butterfly's hierarchical structure.

Another chiral superstructure featuring an azimuthally space-variant surface orientation with a topological defect in the center has attracted extensive attention for its special ability to generate OVs. That is, the CLC *q*-plate containing a screw dislocation in the spatial distribution of the CLC chiral superstructures. Referring to the above principle of the reflective geometric phase, Kobashi et al. demonstrated the high-efficiency, spin-dependent, and polychromatic generation of OVs at a normal incidence (Figure 10b).[149] As a result of the central phase singularity, donut-like reflected diffraction patterns were obtained. For the large-angle oblique incidence, the Bragg band was blueshifted and nearly 100% generation of OVs was achieved without polarization selectivity. Rafayelyan and Brasselet further verified this intrinsic spectrally broadband character of spin–orbit optical phase singularities generation from both diffractive and nondiffractive paraxial light beams.[150] More recently, Nassiri et al. extended the previously introduced concept of the CLC reflective *q*-plate to polychromatic shaping of the radial degrees of freedom of light by combining azimuthal and radial structuring of CLC superstructures, which enabled the generation of high-order Laguerre–Gaussian beams over a broad spectral range.[151] In addition to the CLC flat slabs, Rafayelyan et al. also reported OV generation from self-organized CLC droplets in the Bragg regime that unveiled the spin–orbit consequences of the droplet curvature.[33,152] These
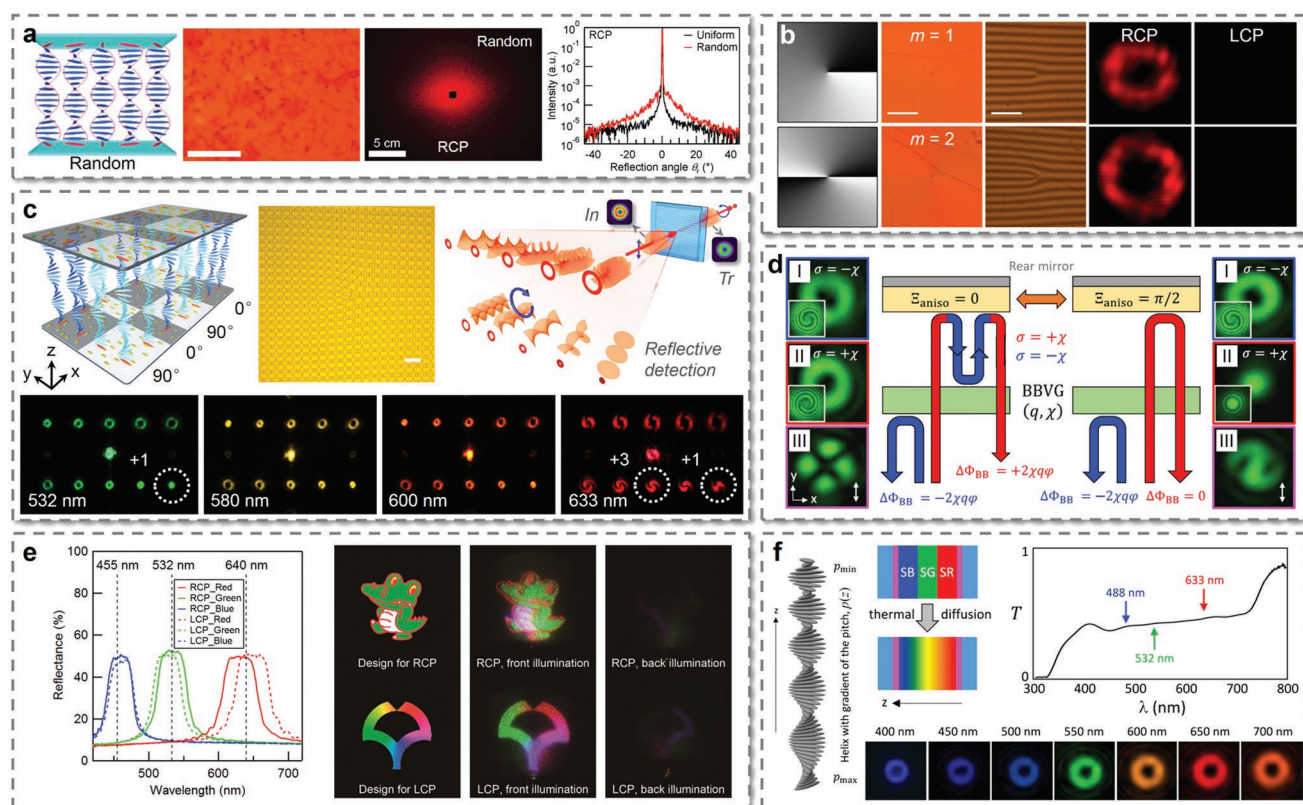
Figure 10. Advanced reflective beam structuring. a) *Morpho*-butterfly-inspired CLC diffuse reflector: schematic diagram of a director distribution with random planar alignment; optical image recorded under the reflection mode of an optical microscope, scale bar: 50 μm; reflection patterns for RCP incidence; angular profile of the reflected light intensity upon a normal RCP incidence. Reproduced with permission.[148] Copyright 2017, Wiley-VCH. b) CLC *q*-plate: director distribution on substrate, polarized micrographs, and measured interferograms at 580 nm with $m = 1$ and $m = 2$, scale bar: 200 μm; corresponding light spots detected by a camera at a normal incidence of RCP and LCP light at 633 nm. Reproduced with permission.[149] Copyright 2016, American Physical Society. c) CLC OV processor: schematic and reflective micrograph, scale bar: 100 μm; schematic illustration for the OV detection, the polarization states of the incident, reflected, and transmitted light are indicated by blue arrows, insets are intensity images of the incident and transmitted OVs; reflected diffraction patterns for different incident OVs and wavelengths. Reproduced with permission.[153] Copyright 2018, Wiley-VCH. d) Mirror-backed CLC *q*-plate with $q = 1$ and $\chi = -1$: on-demand activation of geometric phase beam shaping of the incident light with $\sigma = \chi$ by tuning the birefringent phase delay Ξ_{aniso}; far-field intensity profiles of the reflected light for incident helicity $\sigma = \pm\chi$ and linear polarization after polarization analysis, insets: interference patterns. Reproduced with permission.[155] Copyright 2018, American Physical Society. e) Pseudocolor, chiral-encoded, and double-sided hologram: reflection spectra of the six-layered CLC hologram device, right- and left-handed CLCs with the respective pitch set to operate at red, green, and blue wavelengths; the designed holograms and generated circular-polarization- and illumination-side-dependent far-field images; the front and back illumination correspond to illumination from the side with and without the hologram pattern. Reproduced with permission.[162] Copyright 2017, Nature Publishing Group. f) Ultrabroadband gradient-pitch CLC *q*-plate: illustration of the supramolecular helix with a gradient pitch; sketch of the initial three-layer stack of cholesteric oligomers before and after thermal treatment leading to interdiffusion; typical transmission spectrum of a fabricated gradient-pitch CLC sample under unpolarized illumination; experimental spectral components for far-field intensity profiles from 400 to 700 nm. Reproduced with permission.[160] Copyright 2017, American Physical Society.

results offer a practical solution to the polychromatic management of the OAM of light.

Parallel generation, manipulation, and detection of OVs are a key challenge in OAM-based optical communications and high-dimensional quantum informatics.[107] To address this issue, Chen et al. proposed a concept of digitalized chiral superstructures by encoding a specific binary Dammann vortex grating pattern.[153] As clearly presented in Figure 10c, the designed CLC OV processor is characterized by alternating chiral helixes with a 90° rotation. Up to 25 different OVs were extracted with good energy uniformity and high efficiency over a wide wavelength range of 116 nm. By further emphasizing the spin-determined phase invariance, the multiplexed OVs were detected simultaneously without mode distortion, permitting a

polychromatic, large-capacity, and in situ route for parallel OV processing. Such a multifunctional CLC device provides a satisfactory platform for the OAM incorporated wavelength-division multiplexing, which is expected to dramatically increase the capacity of optical communication systems.[95,154]

However, these broadband benefits are mitigated by the fact that flipping the incident helicity does not ensure geometric phase reversal.[155] Conventional CLC GPOEs cannot process both spin-states at once, in contrast to the transmissive nematic LC elements, which would become a fundamental limitation. Rafayelyan and Brasselet proposed a satisfactory solution by a simple and robust add-on and emphasized its advantages in the context of spin-to-OAM mapping.[155] With the assistance of a rear mirror added to the CLC *q*-plate, polychromatic vector

**ADVANCED
SCIENCE NEWS**

www.advancedsciencenews.com

**ADVANCED
MATERIALS**

www.advmat.de

beams and vectorial vortex beams were achieved by tuning the birefringent phase delay (Figure 10d). Lin et al. reported another strategy via stacking two opposite-handed CLC films with the same pitch and surface azimuthal orientation to generate broadband vector beams.[156] In addition to the simultaneous manipulation of both spin-states in the reflective manner, one can achieve transflective functionalities by integrating the CLC reflective planar optics with nematic LC-mediated transmissive GPOEs. Lin et al. demonstrated a dual-functional multilayer LC *q*-plate, in which both transmitted and reflected light underwent spin-to-OAM conversion.[157] Ono et al. presented a double-layered structure that can modulate the reflective geometric phase twice as much compared with conventional CLC GPOEs.[158] A reflective deflector and an OV generator were fabricated, in which a twofold increase was achieved in the diffraction angle and the topological charge, respectively.

The operating bandwidth of CLC-based reflective planar optics is determined by the birefringence and helical pitch. Typically, it is on the scale of several tens of nanometers in the visible domain. To further extend the working spectral range, gradient-pitch CLC materials can be introduced, which can be achieved by thermal diffusion, slow polymerization of photocurable monomers, and stacking of multiple CLC films with various pitches.[132,159] As revealed in Figure 10f, Rafayelyan et al. adopted thermal treatment to promote the interdiffusion of a three-layer stack of cholesteric oligomers, and thus, fabricated gradient-pitch CLCs imprinted with in-plane space-variant supramolecular helixes.[160] Ultrabroadband OV was generated over the full visible range covering 400–700 nm. Similar results were obtained by Kobashi et al. using a polymer-stabilizable CLC material upon irradiation of weak UV light.[161] Taking advantage of powerful photopatterning technology, more extraordinary chiral hierarchical architectures can be flexibly designed and conveniently fabricated. Kobashi et al. reported a pseudocolor, chiral-encoded, and double-sided hologram by simply stacking six CLC layers containing different patterns for different operation wavelengths, i.e., right- and left-handed CLCs with the pitch set to operate at red, green, and blue wavelengths, respectively (Figure 10e).[162] Different orientation patterns imprinted on two substrates of each single CLC layer resulted in viewing-side-dependent asymmetry of the reconstructed holograms. These unique characteristics make CLC chiral superstructures a promising choice for dynamic holography and optical information encryption.

5.3. Active Geometric Phase

Active planar optical devices that can dynamically manipulate light are highly sought after in numerous fields, but they remain a daunting challenge. Most conventional GPOEs suffer from static functions because their performances are fixed once they are fabricated; hence, they cannot be varied at will. The development of actively tunable geometric phase could potentially unlock a variety of advanced adaptive and multifunctional optical devices, and thus, has attracted ever-growing attention in recent years.[163] Recently, CLCs have been extensively studied in the dynamic tuning of the helical pitch via various external stimuli, including mechanics, temperature, electric

fields, magnetic fields, and light irradiation.[37,164] More intriguingly, the chirality of CLCs is also sensitive to different stimuli, enabling the reversible handedness inversion of CLC superstructures.[36] These intrinsic stimuli-responsive features of self-assembled soft matter will endow CLC GPOEs with abundant dynamic tunability, opening a new frontier in active planar optics with merits of multiple functionalities, broad bandwidth, high compactness, and low loss.

For mechanical tunability, Yin et al. employed polydimethylsiloxane (PDMS) as an elastic substrate with good chemical stability and reasonable transparency, and achieved a stretchable, flexible, and rollable CLC polymer reflective deflector.[165] **Figure 11**a shows its elasto-optic properties, indicating a tunable periodicity with high diffraction efficiency and good repeatability. The corresponding Bragg reflection band and diffraction angle could be dynamically tuned by applying the appropriate strain. The good adhesiveness of PDMS films enables this device to adhere to curved surfaces, facilitating a compact optical system for AR displays.[166] Additionally, thermal control can be utilized for tuning of the working band. Kobashi et al. introduced a temperature-sensitive CLC material with a decreasing pitch along with increasing temperature.[32,167] Accordingly, the Bragg band shifted from the red to the blue region by a temperature change within 10 °C (Figure 11b), allowing the same phase modulation for various colors.

Mechanics- and temperature-based tuning of CLC GPOEs are generally slow. Recently, additional efforts have been devoted to research on the faster electrical switching of those reflective planar optics. Kobashi et al. performed the in situ polymerization in a photopolymerizable CLC system to form a polymer/LC nanocomposite,[168] which narrowed the reflection band under an electric field (Figure 11c).[32] By properly selecting a certain wavelength, on/off switching of the reflective deflection was achieved, and the response time was extremely fast on the order of 100 µs. Similarly, Kowalski et al. fabricated a polymer-stabilized CLC material and imprinted a cubic phase profile, leading to the spectrally tunable generation of Airy beams (Figure 11d).[169] Under both green and red laser illumination, the element was switched to form an Airy beam depending on the electrically tailored reflection band. Moreover, by combing multistimuli-sensitive components, Chen et al. developed a thermally, electrically, and optically responsive self-organized CLC grating.[170] In particular, a dual-frequency CLC was adopted, exhibiting distinguished electrical responses to low- and high-frequency signals (Figure 11e). By applying different electric fields, planar states, homeotropic states, and focal conic states of CLCs alternately appeared, and thus, the Bragg reflection was switched. Low light scattering and rapid switching time were also demonstrated. These works pave the way toward novel smart electro-optical devices.

In contrast to other stimuli, the light control exhibits superiorities of easy operation, noninvasiveness, and remote spatiotemporal resolution, which has always been a research hotspot.[139,171] With the help of a chirality photoinvertible CLC superstructure, Chen et al. proposed a universal strategy for active planar optics with unique features of continuously tunable working spectra and light-flipped functionalities.[172] By flexibly programing the alignment of a CLC doped with a photoresponsive chiral molecular switch and a static dopant
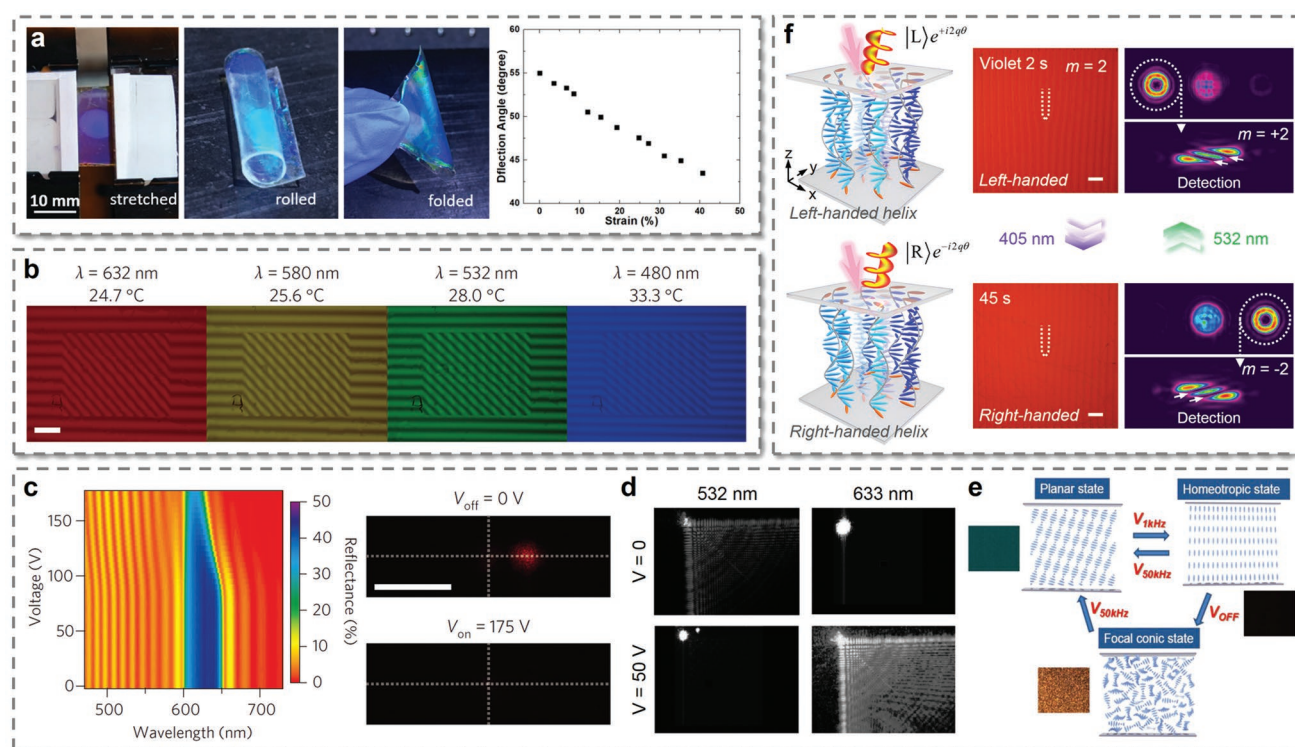
Figure 11. Active planar optics via stimuli-driven chiral superstructures. a) Mechanical tunability: images of the stretched, rolled, and folded sample with a 3 μm thick CLC polymer deflector on a 160 μm thick PDMS substrate; measured diffraction angle at 532 nm under different stretched lengths. Reproduced with permission.[165] Copyright 2019, Optical Society of America. b) Thermal control: temperature-dependent experimental interferograms at different wavelengths of the reflective deflector using a temperature-sensitive CLC material, scale bar: 200 μm. Reproduced with permission.[32] Copyright 2016, Nature Publishing Group. c–e) Electrical switch: c) voltage-dependent reflectance, and a reflected laser spot when switched off and on using a polymer/LC nanocomposite, scale bar: 1 mm. Reproduced with permission.[32] Copyright 2016, Nature Publishing Group. d) Far-field images of the reflection from a polymer-stabilized CLC Airy mask illuminated by a 532 and 633 nm laser at different voltages. Reproduced with permission.[169] Copyright 2019, Optical Society of America. e) Schematic of the working principle of an electrically switchable CLC deflector based on a dual-frequency LC host, and corresponding micrographs in the planar state, homeotropic state, and focal conic state. Reproduced with permission.[170] Copyright 2019, Wiley-VCH. f) Light activation: schematic illustrations of the photoresponsive CLC q-plate before and after light-directed chirality inversion of CLC superstructures; micrographs, reflected diffraction patterns, and corresponding OAM detections of the linearly gradient phase integrated CLC q-plate ($q = 1$) under 2 and 45 s violet light irradiation, scale bar: 100 μm. Reproduced with permission.[172] Copyright 2019, Nature Publishing Group.

with opposite handedness, various light-driven GPOEs, such as deflectors, lens, Airy beam, and OV generators, were presented. Their polychromatic working bands were reversibly tuned in an ultrabroad band over 1000 nm. The chirality inversion triggered facile switching of functionalities, including beam steering, focusing/defocusing, and spin-to-OAM conversion (Figure 11f). These multiple optical functionalities and reversible performances are integrated in a single device via a contactless light stimulus, simultaneously satisfying several key requirements of active planar optics.

6. Conclusion and Outlook

In this review, we have briefly summarized recent advances in the LC-mediated geometric phase. Over the past few years, exciting developments have constantly been witnessed in both nematic LC-mediated transmissive and CLC-mediated broadband reflective planar optics, becoming one of the most attractive topics in the material science and optical scientific community. Particularly, the most recently discovered reflective

geometric phase from CLCs has achieved unprecedented functionalities and is completely compatible with various CLC functionalization strategies. The intrinsic rapid self-organization of LC superstructures makes such elements easy to fabricate, cost and energy efficient, and amenable to bulk production. The exhibited complex and versatile performances cannot be easily achieved with traditional artificial nanostructures. Such research advances our fundamental understanding and the application of soft hierarchical superstructures, improves information displays, optical manipulation, communication, and quantum optics, and even unveils unchartered territories.

Future work might be concentrated on several aspects. First, a more consummate photopatterning technology could be developed that possesses merits of ultrahigh resolution, large-area manufacturing, and time savings. This technology would promote free control of the light wavefront[173] and corresponding practical applications of LC-mediated GPOEs in the industry and our daily life. Second, beyond the visible regime, further exploiting their potentials in the IR, terahertz, and even microwave range is also of great significance. Since absorptive electrodes can be completely avoidable, the optical damage threshold would be

drastically increased, allowing the manipulation of short-pulse intense light. This may inspire applications in light bullets and industrial laser processing.[174] Third, attempt toward new LC phases and materials represent another meaningful topic. For instance, the reflective geometric phase can be achieved in 3D chiral blue phases[175] by controlling the crystal orientation.[143,176] A similar effect could be predicted in the chiral smectic C (SmC*) phase[177] and the heliconical cholesteric phase.[142,178] By further investigating the limited penetration depth of light in helical superstructures, nonreciprocal optics could be reasonably expected. Taking full advantage of the external stimulus response of these soft chiral materials will certainly facilitate the discovery of active and multifunctional optical devices. Undoubtedly, more efforts are still needed to improve the stability, durability, and responsivity. Recent years have also witnessed an emergence in the orientation control of LC phases formed by 2D or discotic nanomaterials, including graphene,[179] graphene oxide,[180] and transition metal dichalcogenides.[181] Through these 2D LCs, even more fantastic devices could be anticipated thanks to their additional degrees of orientational freedom compared to that of rod-like nanostructures. Finally, in addition to all LC-mediated GPOEs, the collaboration of LCs and other man-made nanostructures, such as 2D metasurfaces or 3D metamaterials, is a deep subject with numerous work to come.[7,182] In brief, we believe that research and development of the LC-mediated geometric phase may unlock a variety of intelligent apparatuses and revolutionary applications in the foreseeable future.

Conflict of Interest

The authors declare no conflict of interest.

[1] A. Forbes, A. Dudley, M. McLaren, *Adv. Opt. Photonics* **2016**, *8*, 200.

[2] N. Yu, F. Capasso, *Nat. Mater.* **2014**, *13*, 139.

[3] a) P. Genevet, F. Capasso, F. Aieta, M. Khorasaninejad, R. Devlin, *Optica* **2017**, *4*, 139; b) K. Huang, F. Qin, H. Liu, H. Ye, C. W. Qiu, M. Hong, B. Luk'yanchuk, J. Teng, *Adv. Mater.* **2018**, *30*, 1704556.

[4] a) S. Pancharatnam, *Proc. - Indian Acad. Sci., Sect. A* **1956**, *44*, 247; b) M. V. Berry, *J. Mod. Opt.* **1987**, *34*, 1401; c) Z. E. Bomzon, G. Biener, V. Kleiner, E. Hasman, *Opt. Lett.* **2002**, *27*, 1141.

[5] K. Bliokh, F. Rodríguez-Fortuño, F. Nori, A. V. Zayats, *Nat. Photonics* **2015**, *9*, 796.

[6] S. Chen, Z. Li, Y. Zhang, H. Cheng, J. Tian, *Adv. Opt. Mater.* **2018**, *6*, 1800104.

[7] T. Cui, B. Bai, H. B. Sun, *Adv. Funct. Mater.* **2019**, *29*, 1806692.

[8] D. Wen, F. Yue, W. Liu, S. Chen, X. Chen, *Adv. Opt. Mater.* **2018**, *6*, 1800348.

[9] L. Marrucci, C. Manzo, D. Paparo, *Phys. Rev. Lett.* **2006**, *96*, 163905.

[10] J. Kim, Y. Li, M. N. Miskiewicz, C. Oh, M. W. Kudenov, M. J. Escuti, *Optica* **2015**, *2*, 958.

[11] P. Chen, Y. Q. Lu, W. Hu, *Liq. Cryst.* **2016**, *43*, 2051.

[12] a) G. Li, S. Zhang, T. Zentgraf, *Nat. Rev. Mater.* **2017**, *2*, 17010; b) V. C. Su, C. H. Chu, G. Sun, D. P. Tsai, *Opt. Express* **2018**, *26*, 13148; c) S. Chen, Z. Li, W. Liu, H. Cheng, J. Tian, *Adv. Mater.* **2019**, *31*, 1802458.

[13] W. Wan, J. Gao, X. Yang, *Adv. Opt. Mater.* **2017**, *5*, 1700541.

[14] Y. H. Kim, D. K. Yoon, H. S. Jeong, O. D. Lavrentovich, H. T. Jung, *Adv. Funct. Mater.* **2011**, *21*, 610.

[15] I. C. Khoo, S. T. Wu, *Optics and Nonlinear Optics of Liquid Crystals*, World Scientific, Singapore **1993**.

[16] P. G. de Gennes, J. Prost, *The Physics of Liquid Crystals*, Oxford University Press, New York **1993**.

[17] P. Yeh, C. Gu, *Optics of Liquid Crystal Displays*, Wiley, New York **1999**.

[18] a) D. K. Yang, S. T. Wu, *Fundamentals of Liquid Crystal Devices*, Wiley, Chichester, UK **2006**; b) M. Schadt, *Liq. Cryst.* **2015**, *42*, 646; c) H. W. Chen, R. D. Zhu, J. He, W. Duan, W. Hu, Y. Q. Lu, M. C. Li, S. L. Lee, Y. J. Dong, S. T. Wu, *Light: Sci. Appl.* **2017**, *6*, e17043; d) H. W. Chen, J. H. Lee, B. Y. Lin, S. Chen, S. T. Wu, *Light: Sci. Appl.* **2018**, *7*, 17168.

[19] Z. Zhang, Z. You, D. Chu, *Light: Sci. Appl.* **2014**, *3*, e213.

[20] H. S. Kitzerow, *Liq. Cryst.* **1994**, *16*, 1.

[21] M. Stalder, M. Schadt, *Opt. Lett.* **1996**, *21*, 1948.

[22] a) J. H. Kim, M. Yoneya, H. Yokoyama, *Nature* **2002**, *420*, 159; b) S. Varghese, S. Narayanankutty, C. W. M. Bastiaansen, G. P. Crawford, D. J. Broer, *Adv. Mater.* **2004**, *16*, 1600.

[23] M. Schadt, K. Schmitt, V. Kozinkov, V. Chigrinov, *Jpn. J. Appl. Phys.* **1992**, *31*, 2155.

[24] M. Schadt, H. Seiberle, A. Schuster, *Nature* **1996**, *381*, 212.

[25] V. G. Chigrinov, V. M. Kozenkov, H. S. Kwok, *Photoalignment of Liquid Crystalline Materials: Physics and Applications*, Wiley, Chichester, UK **2008**.

[26] L. Blinov, *Liq. Cryst.* **1999**, *26*, 427.

[27] C. Provenzano, P. Pagliusi, G. Cipparrone, *Appl. Phys. Lett.* **2006**, *89*, 121105.

[28] a) C. Culbreath, N. Glazar, H. Yokoyama, *Rev. Sci. Instrum.* **2011**, *82*, 126107; b) B. Y. Wei, W. Hu, Y. Ming, F. Xu, S. Rubin, J. G. Wang, V. Chigrinov, Y. Q. Lu, *Adv. Mater.* **2014**, *26*, 1590.

[29] L. De Sio, D. E. Roberts, Z. Liao, S. Nersisyan, O. Uskova, L. Wickboldt, N. Tabiryan, D. M. Steeves, B. R. Kimball, *Opt. Express* **2016**, *24*, 18297.

[30] Y. Guo, M. Jiang, C. Peng, K. Sun, O. Yaroshchuk, O. Lavrentovich, Q. H. Wei, *Adv. Mater.* **2016**, *28*, 2353.

[31] K. Hisano, M. Aizawa, M. Ishizu, Y. Kurata, W. Nakano, N. Akamatsu, C. J. Barrett, A. Shishido, *Sci. Adv.* **2017**, *3*, e1701610.

[32] J. Kobashi, H. Yoshida, M. Ozaki, *Nat. Photonics* **2016**, *10*, 389.

[33] M. Rafayelyan, G. Tkachenko, E. Brasselet, *Phys. Rev. Lett.* **2016**, *116*, 253902.

[34] R. Barboza, U. Bortolozzo, M. G. Clerc, S. Residori, *Phys. Rev. Lett.* **2016**, *117*, 053903.

[35] H. K. Bisoyi, Q. Li, *Chem. Rev.* **2016**, *116*, 15089.

**ADVANCED
SCIENCE NEWS**

www.advancedsciencenews.com

**ADVANCED
MATERIALS**

www.advmat.de

[36] H. K. Bisoyi, Q. Li, *Angew. Chem., Int. Ed.* **2016**, *55*, 2994.

[37] a) H. K. Bisoyi, T. J. Bunning, Q. Li, *Adv. Mater.* **2018**, *30*, 1706512; b) L. Wang, A. M. Urbas, Q. Li, *Adv. Mater.* **2018**, *30*, 1801335.

[38] C. Zhou, L. Liu, *Appl. Opt.* **1995**, *34*, 5961.

[39] a) X. Yin, Z. Ye, J. Rho, Y. Wang, X. Zhang, *Science* **2013**, *339*, 1405; b) X. Ling, X. Zhou, K. Huang, Y. Liu, C. W. Qiu, H. Luo, S. Wen, *Rep. Prog. Phys.* **2017**, *80*, 066401.

[40] X. Ling, X. Zhou, X. Yi, W. Shu, Y. Liu, S. Chen, H. Luo, S. Wen, D. Fan, *Light: Sci. Appl.* **2015**, *4*, e290.

[41] a) R. C. Devlin, A. Ambrosio, N. A. Rubin, J. B. Mueller, F. Capasso, *Science* **2017**, *358*, 896; b) E. Maguid, M. Yannai, A. Faerman, I. Yulevich, V. Kleiner, E. Hasman, *Science* **2017**, *358*, 1411.

[42] L. Marrucci, C. Manzo, D. Paparo, *Appl. Phys. Lett.* **2006**, *88*, 221102.

[43] C. Peng, T. Turiv, Y. Guo, Q. H. Wei, O. D. Lavrentovich, *Science* **2016**, *354*, 882.

[44] M. Wang, Y. Li, H. Yokoyama, *Nat. Commun.* **2017**, *8*, 388.

[45] a) A. K. Srivastava, W. Zhang, J. Schneider, A. L. Rogach, V. G. Chigrinov, H. S. Kwok, *Adv. Mater.* **2017**, *29*, 1701091; b) L. L. Ma, M. J. Tang, W. Hu, Z. Q. Cui, S. J. Ge, P. Chen, L. J. Chen, H. Qian, L. F. Chi, Y. Q. Lu, *Adv. Mater.* **2017**, *29*, 1606671; c) L. L. Ma, W. Hu, Z. G. Zheng, S. B. Wu, P. Chen, Q. Li, Y. Q. Lu, *Adv. Opt. Mater.* **2019**, *7*, 1900393.

[46] H. Akiyama, T. Kawara, H. Takada, H. Takatsu, V. Chigrinov, E. Prudnikova, V. Kozenkov, H. Kwok, *Liq. Cryst.* **2002**, *29*, 1321.

[47] a) V. Chigrinov, A. Muravski, H. S. Kwok, H. Takada, H. Akiyama, H. Takatsu, *Phys. Rev. E* **2003**, *68*, 061702; b) V. Chigrinov, S. Pikin, A. Verevochnikov, V. Kozenkov, M. Khazimullin, J. Ho, D. D. Huang, H. S. Kwok, *Phys. Rev. E* **2004**, *69*, 061713.

[48] T. Zhan, Y. H. Lee, G. Tan, J. Xiong, K. Yin, F. Gou, J. Zou, N. Zhang, D. Zhao, J. Yang, S. Liu, S. T. Wu, *J. Opt. Soc. Am. B* **2019**, *36*, D52.

[49] a) Y. Y. Tzeng, S. W. Ke, C. L. Ting, A. Y. G. Fuh, T. H. Lin, *Opt. Express* **2008**, *16*, 3768; b) S. Nersisyan, N. Tabiryan, D. M. Steeves, B. R. Kimball, *Opt. Express* **2009**, *17*, 11926; c) Y. H. Huang, S. W. Ko, M. S. Li, S. C. Chu, A. Y. G. Fuh, *Opt. Express* **2013**, *21*, 10954.

[50] S. Slussarenko, A. Murauski, T. Du, V. Chigrinov, L. Marrucci, E. Santamato, *Opt. Express* **2011**, *19*, 4085.

[51] F. Fan, T. Du, A. K. Srivastava, W. Lu, V. Chigrinov, H. S. Kwok, *Opt. Express* **2012**, *20*, 23036.

[52] H. Yoshida, K. Asakura, J. Fukuda, M. Ozaki, *Nat. Commun.* **2015**, *6*, 7180.

[53] a) C. Peng, Y. Guo, T. Turiv, M. Jiang, Q. H. Wei, O. D. Lavrentovich, *Adv. Mater.* **2017**, *29*, 1606112; b) M. Jiang, H. Yu, X. Feng, Y. Guo, I. Chaganava, T. Turiv, O. D. Lavrentovich, Q. H. Wei, *Adv. Opt. Mater.* **2018**, *6*, 1800961.

[54] H. Yu, M. Jiang, Y. Guo, T. Turiv, W. Lu, V. Ray, O. D. Lavrentovich, Q. H. Wei, *Adv. Opt. Mater.* **2019**, *7*, 1900117.

[55] M. Jiang, Y. Guo, H. Yu, Z. Zhou, T. Turiv, O. D. Lavrentovich, Q. H. Wei, *Adv. Mater.* **2019**, *31*, 1808028.

[56] A. M. Tam, F. Fan, T. Du, W. Hu, W. Zhang, C. Zhao, X. Wang, K. L. Ching, G. Li, H. Luo, V. G. Chigrinov, S. Wen, H. S. Kwok, *Phys. Rev. Appl.* **2017**, *7*, 034010.

[57] M. N. Miskiewicz, M. J. Escuti, *Opt. Express* **2014**, *22*, 12691.

[58] T. H. Ware, M. E. McConney, J. J. Wie, V. P. Tondiglia, T. J. White, *Science* **2015**, *347*, 982.

[59] a) H. Wu, W. Hu, H. C. Hu, X. W. Lin, G. Zhu, J. W. Choi, V. Chigrinov, Y. Q. Lu, *Opt. Express* **2012**, *20*, 16684; b) B. Y. Wei, P. Chen, S. J. Ge, L. C. Zhang, W. Hu, Y. Q. Lu, *Photonics Res.* **2016**, *4*, 70.

[60] P. Chen, B. Y. Wei, W. Ji, S. J. Ge, W. Hu, F. Xu, V. Chigrinov, Y. Q. Lu, *Photonics Res.* **2015**, *3*, 133.

[61] M. Aizawa, M. Ota, K. Hisano, N. Akamatsu, T. Sasaki, C. J. Barrett, A. Shishido, *J. Opt. Soc. Am. B* **2019**, *36*, D47.

[62] Y. Li, Y. Liu, S. Li, P. Zhou, T. Zhan, Q. Chen, Y. Su, S. T. Wu, *Opt. Express* **2019**, *27*, 9054.

[63] a) J. Kim, *Ph.D. Dissertation*, North Carolina State University **2011**; b) J. Kim, C. Oh, S. Serati, M. J. Escuti, *Appl. Opt.* **2011**, *50*, 2636.

[64] a) G. Cipparrone, A. Mazzulla, G. Russo, *Appl. Phys. Lett.* **2001**, *78*, 1186; b) A. Mazzulla, P. Pagliusi, C. Provenzano, G. Russo, G. Carbone, G. Cipparrone, *Appl. Phys. Lett.* **2004**, *85*, 2505.

[65] a) H. Ono, A. Emoto, F. Takahashi, N. Kawatsuki, T. Hasegawa, *J. Appl. Phys.* **2003**, *94*, 1298; b) N. Kawatsuki, T. Hasegawa, H. Ono, T. Tamoto, *Adv. Mater.* **2003**, *15*, 991.

[66] V. Presnyakov, K. Asatryan, T. Galstian, V. Chigrinov, *Opt. Express* **2006**, *14*, 10558.

[67] R. Komanduri, M. Escuti, *Appl. Phys. Lett.* **2009**, *95*, 091106.

[68] W. Duan, P. Chen, B. Y. Wei, S. J. Ge, X. Liang, W. Hu, Y. Q. Lu, *Opt. Mater. Express* **2016**, *6*, 597.

[69] a) Q. Guo, L. Xu, J. Sun, X. Yang, H. Liu, K. Yan, H. Zhao, V. Chigrinov, H. Kwok, *Liq. Cryst.* **2019**, *46*, 1383; b) A. Srivastava, W. Hu, V. Chigrinov, A. Kiselev, Y. Q. Lu, *Appl. Phys. Lett.* **2012**, *101*, 031112.

[70] a) C. Provenzano, P. Pagliusi, G. Cipparrone, *Opt. Express* **2007**, *15*, 5872; b) U. Ruiz, P. Pagliusi, C. Provenzano, V. P. Shibaev, G. Cipparrone, *Adv. Funct. Mater.* **2012**, *22*, 2964; c) Y. Shi, Y. J. Liu, F. Song, V. G. Chigrinov, H. S. Kwok, M. Hu, D. Luo, X. W. Sun, *Opt. Express* **2018**, *26*, 7683; d) I. Nys, J. Beeckman, K. Neyts, *Soft Matter* **2015**, *11*, 7802; e) I. Nys, V. Nersesyan, J. Beeckman, K. Neyts, *Soft Matter* **2018**, *14*, 6892.

[71] Y. Shi, Y. Lai, Y. J. Liu, V. G. Chigrinov, H. S. Kwok, M. Hu, D. Luo, X. W. Sun, *Opt. Express* **2019**, *27*, 13061.

[72] H. Magallanes, E. Brasselet, *Nat. Photonics* **2018**, *12*, 461.

[73] a) C. Zhao, F. Fan, T. Du, V. Chigrinov, H. Kwok, *Opt. Lett.* **2015**, *40*, 2993; b) T. Du, F. Fan, A. M. W. Tam, J. Sun, V. Chigrinov, H. S. Kwok, *Adv. Mater.* **2015**, *27*, 7191.

[74] T. Sasaki, A. Hatayama, A. Emoto, H. Ono, N. Kawatsuki, *J. Appl. Phys.* **2006**, *100*, 063502.

[75] S. R. Nersisyan, N. V. Tabiryan, L. Hoke, D. M. Steeves, B. Kimball, *Opt. Express* **2009**, *17*, 1817.

[76] a) C. Oh, M. J. Escuti, *Opt. Lett.* **2008**, *33*, 2287; b) M. W. Kudenov, M. Miskiewicz, N. Sanders, M. J. Escuti, *Opt. Lett.* **2016**, *41*, 4461; c) K. Gao, C. McGinty, H. Payson, S. Berry, J. Vornehm, V. Finnemeyer, B. Roberts, P. Bos, *Opt. Express* **2017**, *25*, 6283.

[77] C. Peng, T. Turiv, Y. Guo, S. V. Shiyanovskii, Q. H. Wei, O. D. Lavrentovich, *Sci. Adv.* **2016**, *2*, e1600932.

[78] H. Chen, Y. Weng, D. Xu, N. V. Tabiryan, S. T. Wu, *Opt. Express* **2016**, *24*, 7287.

[79] a) T. Zhan, Y. H. Lee, S. T. Wu, *Opt. Express* **2018**, *26*, 4863; b) Y. H. Lin, Y. J. Wang, V. Reshetnyak, *Liq. Cryst. Rev.* **2017**, *5*, 111.

[80] a) U. Ruiz, C. Provenzano, P. Pagliusi, G. Cipparrone, *Opt. Lett.* **2012**, *37*, 4958; b) K. Gao, H. H. Cheng, A. K. Bhowmik, P. J. Bos, *Opt. Express* **2015**, *23*, 26086; c) K. Gao, H. H. Cheng, A. Bhowmik, C. McGinty, P. Bos, *Appl. Opt.* **2016**, *55*, 1145.

[81] Z. He, Y. H. Lee, R. Chen, D. Chanda, S. T. Wu, *Opt. Lett.* **2018**, *43*, 5062.

[82] Z. He, G. Tan, D. Chanda, S. T. Wu, *Opt. Express* **2019**, *27*, 11472.

[83] N. V. Tabiryan, S. V. Serak, D. E. Roberts, D. M. Steeves, B. R. Kimball, *Opt. Express* **2015**, *23*, 25783.

[84] N. V. Tabiryan, S. V. Serak, S. R. Nersisyan, D. E. Roberts, B. Y. Zeldovich, D. M. Steeves, B. R. Kimball, *Opt. Express* **2016**, *24*, 7091.

[85] T. Zhan, J. Xiong, Y. H. Lee, S. T. Wu, *Opt. Express* **2018**, *26*, 35026.

[86] a) Y. Zhou, Y. Yin, Y. Yuan, T. Lin, H. Huang, L. Yao, X. Wang, A. M. Tam, F. Fan, S. Wen, *Liq. Cryst.* **2019**, *46*, 995; b) J. Ren, W. Wang, W. Yang, C. Yuan, K. Zhou, X. Li, A. M. Tam, C. Meng, J. Sun, V. G. Chigrinov, H. Kwok, X. Wang, Z. Zheng, D. Shen, *Chin. Opt. Lett.* **2018**, *16*, 062301.

**ADVANCED
SCIENCE NEWS**

www.advancedsciencenews.com

**ADVANCED
MATERIALS**

www.advmat.de

[87] Y. Ma, A. M. Tam, X. Gan, L. Shi, A. Srivastava, V. Chigrinov, H. Kwok, J. Zhao, *Opt. Express* **2019**, *27*, 10079.

[88] W. Duan, P. Chen, S. J. Ge, X. Liang, W. Hu, *Crystals* **2019**, *9*, 111.

[89] S. Slussarenko, A. Alberucci, C. P. Jisha, B. Piccirillo, E. Santamato, G. Assanto, L. Marrucci, *Nat. Photonics* **2016**, *10*, 571.

[90] C. P. Jisha, A. Alberucci, J. Beeckman, S. Nolte, *Phys. Rev. X* **2019**, *9*, 021051.

[91] a) S. Franke-Arnold, L. Allen, M. Padgett, *Laser Photonics Rev.* **2008**, *2*, 299; b) A. M. Yao, M. J. Padgett, *Adv. Opt. Photonics* **2011**, *3*, 161.

[92] L. Allen, M. W. Beijersbergen, R. Spreeuw, J. Woerdman, *Phys. Rev. A* **1992**, *45*, 8185.

[93] M. Padgett, R. Bowman, *Nat. Photonics* **2011**, *5*, 343.

[94] L. Yan, P. Gregg, E. Karimi, A. Rubano, L. Marrucci, R. Boyd, S. Ramachandran, *Optica* **2015**, *2*, 900.

[95] A. E. Willner, H. Huang, Y. Yan, Y. Ren, N. Ahmed, G. Xie, C. Bao, L. Li, Y. Cao, Z. Zhao, J. Wang, M. P. J. Lavery, M. Tur, S. Ramachandran, A. F. Molisch, N. Ashrafi, S. Ashrafi, *Adv. Opt. Photonics* **2015**, *7*, 66.

[96] a) L. Chen, J. Lei, J. Romero, *Light: Sci. Appl.* **2014**, *3*, e153; b) X. L. Wang, X. D. Cai, Z. E. Su, M. C. Chen, D. Wu, L. Li, N. L. Liu, C. Y. Lu, J. W. Pan, *Nature* **2015**, *518*, 516; c) M. Erhard, R. Fickler, M. Krenn, A. Zeilinger, *Light: Sci. Appl.* **2018**, *7*, 17146.

[97] J. H. Lee, G. Foo, E. G. Johnson, G. A. Swartzlander Jr., *Phys. Rev. Lett.* **2006**, *97*, 053901.

[98] L. Marrucci, E. Karimi, S. Slussarenko, B. Piccirillo, E. Santamato, E. Nagali, F. Sciarrino, *J. Opt.* **2011**, *13*, 064001.

[99] a) F. Cardano, E. Karimi, S. Slussarenko, L. Marrucci, C. de Lisio, E. Santamato, *Appl. Opt.* **2012**, *51*, C1; b) D. Naidoo, F. S. Roux, A. Dudley, I. Litvin, B. Piccirillo, L. Marrucci, A. Forbes, *Nat. Photonics* **2016**, *10*, 327.

[100] Q. Zhan, *Adv. Opt. Photonics* **2009**, *1*, 1.

[101] E. Karimi, B. Piccirillo, E. Nagali, L. Marrucci, E. Santamato, *Appl. Phys. Lett.* **2009**, *94*, 231124.

[102] a) W. Ji, C. H. Lee, P. Chen, W. Hu, Y. Ming, L. Zhang, T. H. Lin, V. Chigrinov, Y. Q. Lu, *Sci. Rep.* **2016**, *6*, 25528; b) P. Chen, W. Ji, B. Y. Wei, W. Hu, V. Chigrinov, Y. Q. Lu, *Appl. Phys. Lett.* **2015**, *107*, 241102; c) Y. Ming, P. Chen, W. Ji, B. Y. Wei, C. H. Lee, T. H. Lin, W. Hu, Y. Q. Lu, *npj Quantum Mater.* **2017**, *2*, 6; d) Z. H. Zhu, P. Chen, L. W. Sheng, Y. L. Wang, W. Hu, Y. Q. Lu, W. Gao, *Appl. Phys. Lett.* **2017**, *110*, 141104; e) Y. Liu, H. Liang, C. W. Chen, X. Xie, W. Hu, P. Chen, J. Wen, J. Zhou, T. H. Lin, I. C. Khoo, *Opt. Express* **2018**, *26*, 28818.

[103] Y. Li, J. Kim, M. J. Escuti, *Appl. Opt.* **2012**, *51*, 8236.

[104] W. Duan, P. Chen, S. J. Ge, B. Y. Wei, W. Hu, Y. Q. Lu, *Opt. Express* **2017**, *25*, 14059.

[105] P. Chen, S. J. Ge, W. Duan, B. Y. Wei, G. X. Cui, W. Hu, Y. Q. Lu, *ACS Photonics* **2017**, *4*, 1333.

[106] a) H. Dammann, E. Klotz, *J. Mod. Opt.* **1977**, *24*, 505; b) S. J. Ge, P. Chen, L. L. Ma, Z. Liu, Z. G. Zheng, D. Shen, W. Hu, Y. Q. Lu, *Opt. Mater. Express* **2016**, *6*, 1087; c) P. Chen, S. J. Ge, L. L. Ma, W. Hu, V. Chigrinov, Y. Q. Lu, *Phys. Rev. Appl.* **2016**, *5*, 044009.

[107] T. Lei, M. Zhang, Y. R. Li, P. Jia, G. N. Liu, X. G. Xu, Z. H. Li, C. J. Min, J. Lin, C. Y. Yu, H. B. Niu, X. C. Yuan, *Light: Sci. Appl.* **2015**, *4*, e257.

[108] R. Xu, P. Chen, J. Tang, W. Duan, S. J. Ge, L. L. Ma, R. X. Wu, W. Hu, Y. Q. Lu, *Phys. Rev. Appl.* **2018**, *10*, 034061.

[109] a) M. J. Tang, P. Chen, W. L. Zhang, A. M. Tam, V. G. Chigrinov, W. Hu, Y. Q. Lu, *Opt. Express* **2016**, *24*, 25510; b) S. Delaney, M. M. Sánchez-López, I. Moreno, J. A. Davis, *Appl. Opt.* **2017**, *56*, 596; c) S. Lou, Y. Zhou, Y. Yuan, T. Lin, F. Fan, X. Wang, H. Huang, S. Wen, *Opt. Express* **2019**, *27*, 8596.

[110] a) L. Wang, X. W. Lin, W. Hu, G. H. Shao, P. Chen, L. J. Liang, B. B. Jin, P. H. Wu, H. Qian, Y. N. Lu, X. Liang, Z. G. Zheng, Y. Q. Lu, *Light: Sci. Appl.* **2015**, *4*, e253; b) S. Ge, P. Chen, Z. Shen, W. Sun, X. Wang, W. Hu, Y. Zhang, Y. Lu, *Opt. Express* **2017**, *25*, 12349; c) S. J. Ge, Z. X. Shen, P. Chen, X. Liang, X. K. Wang, W. Hu, Y. Zhang, Y. Q. Lu, *Crystals* **2017**, *7*, 314.

[111] R. Barboza, U. Bortolozzo, M. Clerc, S. Residori, E. Vidal-Henriquez, *Adv. Opt. Photonics* **2015**, *7*, 635.

[112] E. Brasselet, N. Murazawa, H. Misawa, S. Juodkazis, *Phys. Rev. Lett.* **2009**, *103*, 103903.

[113] a) E. Brasselet, *Phys. Rev. Lett.* **2012**, *108*, 087801; b) Y. Sasaki, V. Jampani, C. Tanaka, N. Sakurai, S. Sakane, K. V. Le, F. Araoka, H. Orihara, *Nat. Commun.* **2016**, *7*, 13238; c) Y. Sasaki, M. Ueda, K. V. Le, R. Amano, S. Sakane, S. Fujii, F. Araoka, H. Orihara, *Adv. Mater.* **2017**, *29*, 1703054.

[114] M. G. Nassiri, E. Brasselet, *Phys. Rev. Lett.* **2018**, *121*, 213901.

[115] P. Salamon, N. Éber, Y. Sasaki, H. Orihara, Á. Buka, F. Araoka, *Phys. Rev. Appl.* **2018**, *10*, 044008.

[116] a) G. Ruffato, E. Brasselet, M. Massari, F. Romanato, *Appl. Phys. Lett.* **2018**, *113*, 011109; b) E. Brasselet, *Phys. Rev. Lett.* **2018**, *121*, 033901.

[117] C. Loussert, U. Delabre, E. Brasselet, *Phys. Rev. Lett.* **2013**, *111*, 037802.

[118] a) R. Barboza, U. Bortolozzo, G. Assanto, E. Vidal-Henriquez, M. Clerc, S. Residori, *Phys. Rev. Lett.* **2012**, *109*, 143901; b) R. Barboza, U. Bortolozzo, G. Assanto, E. Vidal-Henriquez, M. Clerc, S. Residori, *Phys. Rev. Lett.* **2013**, *111*, 093902.

[119] A. Aleksanyan, N. Kravets, E. Brasselet, *Phys. Rev. Lett.* **2017**, *118*, 203902.

[120] a) L. T. De Haan, C. Sánchez-Somolinos, C. M. Bastiaansen, A. P. Schenning, D. J. Broer, *Angew. Chem., Int. Ed.* **2012**, *51*, 12469; b) M. E. McConney, A. Martinez, V. P. Tondiglia, K. M. Lee, D. Langley, I. I. Smalyukh, T. J. White, *Adv. Mater.* **2013**, *25*, 5880; c) H. Zeng, O. M. Wani, P. Wasylczyk, R. Kaczmarek, A. Priimagi, *Adv. Mater.* **2017**, *29*, 1701814; d) G. Babakhanova, T. Turiv, Y. Guo, M. Hendrikx, Q. H. Wei, A. P. Schenning, D. J. Broer, O. D. Lavrentovich, *Nat. Commun.* **2018**, *9*, 456.

[121] N. K. Efremidis, Z. Chen, M. Segev, D. N. Christodoulides, *Optica* **2019**, *6*, 686.

[122] G. Siviloglou, J. Broky, A. Dogariu, D. Christodoulides, *Phys. Rev. Lett.* **2007**, *99*, 213901.

[123] a) M. Gecevičius, M. Beresna, R. Drevinskas, P. G. Kazansky, *Opt. Lett.* **2014**, *39*, 6791; b) T. Cerda, U. Ruiz, P. Pagliusi, G. Cipparrone, *J. Opt. Soc. Am. B* **2019**, *36*, D103.

[124] B. Y. Wei, P. Chen, W. Hu, W. Ji, L. Y. Zheng, S. J. Ge, Y. Ming, V. Chigrinov, Y. Q. Lu, *Sci. Rep.* **2015**, *5*, 17484.

[125] B. Y. Wei, P. Chen, S. J. Ge, W. Duan, W. Hu, Y. Q. Lu, *Appl. Phys. Lett.* **2016**, *109*, 121105.

[126] B. Y. Wei, S. Liu, P. Chen, S. X. Qi, Y. Zhang, W. Hu, Y. Q. Lu, J. L. Zhao, *Appl. Phys. Lett.* **2018**, *112*, 121101.

[127] U. Ruiz, P. Pagliusi, C. Provenzano, K. Volke-Sepúlveda, G. Cipparrone, *Opt. Express* **2013**, *21*, 7505.

[128] H. Larocque, J. Gagnon-Bischoff, F. Bouchard, R. Fickler, J. Upham, R. W. Boyd, E. Karimi, *J. Opt.* **2016**, *18*, 124002.

[129] L. A. Alemán-Castaneda, B. Piccirillo, E. Santamato, L. Marrucci, M. A. Alonso, *Optica* **2019**, *6*, 396.

[130] a) G. C. Berkhout, M. P. Lavery, J. Courtial, M. W. Beijersbergen, M. J. Padgett, *Phys. Rev. Lett.* **2010**, *105*, 153601; b) H. Larocque, J. Gagnon-Bischoff, D. Mortimer, Y. Zhang, F. Bouchard, J. Upham, V. Grillo, R. W. Boyd, E. Karimi, *Opt. Express* **2017**, *25*, 19832; c) G. F. Walsh, L. De Sio, D. E. Roberts, N. Tabiryan, F. J. Aranda, B. R. Kimball, *Opt. Lett.* **2018**, *43*, 2256; d) S. Zheng, Y. Li, Q. Lin, X. Zeng, G. Zheng, Y. Cai, Z. Chen, S. Xu, D. Fan, *Photonics Res.* **2018**, *6*, 385; e) J. Fang, Z. Xie, T. Lei, C. Min, L. Du, Z. Li, X. Yuan, *ACS Photonics* **2018**, *5*, 3478.

[131] a) V. Sharma, M. Crne, J. O. Park, M. Srinivasarao, *Science* **2009**, *325*, 449; b) J. C. Weaver, G. W. Milliron, A. Miserez, K. Evans-Lutterodt, S. Herrera, I. Gallana, W. J. Mershon, B. Swanson, P. Zavattieri,

E. DiMasi, D. Kisailus, *Science* **2012**, *336*, 1275; c) B. D. Wilts, H. M. Whitney, B. J. Glover, U. Steiner, S. Vignolini, *Mater. Today: Proc.* **2014**, *1*, 177; d) M. Mitov, *Soft Matter* **2017**, *13*, 4176.

[132] M. Mitov, *Adv. Mater.* **2012**, *24*, 6260.

[133] I. Dierking, *Textures of Liquid Crystals*, Wiley, Weinheim, Germany **2003**.

[134] M. Faryad, A. Lakhtakia, *Adv. Opt. Photonics* **2014**, *6*, 225.

[135] A. Ryabchun, A. Bobrovsky, *Adv. Opt. Mater.* **2018**, *6*, 1800335.

[136] a) S. T. Wu, D. K. Yang, *Reflective Liquid Crystal Displays*, Wiley, New York **2001**; b) J. Li, H. K. Bisoyi, J. Tian, J. Guo, Q. Li, *Adv. Mater.* **2019**, *31*, 1807751.

[137] a) Y. Wang, Q. Li, *Adv. Mater.* **2012**, *24*, 1926; b) L. Qin, W. Gu, J. Wei, Y. Yu, *Adv. Mater.* **2018**, *30*, 1704941; c) M. Schwartz, G. Lenzini, Y. Geng, P. B. Rønne, P. Y. Ryan, J. P. Lagerwall, *Adv. Mater.* **2018**, *30*, 1707382.

[138] a) H. C. Jau, Y. Li, C. C. Li, C. W. Chen, C. T. Wang, H. K. Bisoyi, T. H. Lin, T. J. Bunning, Q. Li, *Adv. Opt. Mater.* **2015**, *3*, 166; b) L. L. Ma, S. S. Li, W. S. Li, W. Ji, B. Luo, Z. G. Zheng, Z. P. Cai, V. Chigrinov, Y. Q. Lu, W. Hu, L. J. Chen, *Adv. Opt. Mater.* **2015**, *3*, 1691.

[139] a) A. Ryabchun, A. Bobrovsky, J. Stumpe, V. Shibaev, *Adv. Opt. Mater.* **2015**, *3*, 1273; b) Z. G. Zheng, Y. Li, H. K. Bisoyi, L. Wang, T. J. Bunning, Q. Li, *Nature* **2016**, *531*, 352.

[140] a) R. Eelkema, M. M. Pollard, J. Vicario, N. Katsonis, B. S. Ramon, C. W. Bastiaansen, D. J. Broer, B. L. Feringa, *Nature* **2006**, *440*, 163; b) Y. Li, E. Prince, S. Cho, A. Salari, Y. M. Golestani, O. D. Lavrentovich, E. Kumacheva, *Proc. Natl. Acad. Sci. USA* **2017**, *114*, 2137.

[141] H. Coles, S. Morris, *Nat. Photonics* **2010**, *4*, 676.

[142] J. Xiang, A. Varanytsia, F. Minkowski, D. A. Paterson, J. M. Storey, C. T. Imrie, O. D. Lavrentovich, P. Palffy-Muhoray, *Proc. Natl. Acad. Sci. USA* **2016**, *113*, 12925.

[143] H. Yoshida, J. Kobashi, *Liq. Cryst.* **2016**, *43*, 1909.

[144] J. Kobashi, Y. Mohri, H. Yoshida, M. Ozaki, *Opt. Data Process. Storage* **2017**, *3*, 61.

[145] Y. Weng, D. Xu, Y. Zhang, X. Li, S. T. Wu, *Opt. Express* **2016**, *24*, 17746.

[146] a) Y. H. Lee, K. Yin, S. T. Wu, *Opt. Express* **2017**, *25*, 27008; b) Y. Weng, Y. Zhang, J. Cui, A. Liu, Z. Shen, X. Li, B. Wang, *Opt. Lett.* **2018**, *43*, 5773.

[147] S. V. Serak, D. E. Roberts, J. Y. Hwang, S. R. Nersisyan, N. V. Tabiryan, T. J. Bunning, D. M. Steeves, B. R. Kimball, *J. Opt. Soc. Am. B* **2017**, *34*, B56.

[148] Y. Mohri, J. Kobashi, H. Yoshida, M. Ozaki, *Adv. Opt. Mater.* **2017**, *5*, 1601071.

[149] J. Kobashi, H. Yoshida, M. Ozaki, *Phys. Rev. Lett.* **2016**, *116*, 253903.

[150] M. Rafayelyan, E. Brasselet, *Opt. Lett.* **2016**, *41*, 3972.

[151] M. G. Nassiri, S. Y. Cho, H. Yoshida, M. Ozaki, E. Brasselet, *Phys. Rev. A* **2018**, *98*, 063834.

[152] G. Tkachenko, M. Rafayelyan, E. Brasselet, *Phys. Rev. A* **2017**, *95*, 053839.

[153] P. Chen, L. L. Ma, W. Duan, J. Chen, S. J. Ge, Z. H. Zhu, M. J. Tang, R. Xu, W. Gao, T. Li, W. Hu, Y. Q. Lu, *Adv. Mater.* **2018**, *30*, 1705865.

[154] J. Wang, J. Y. Yang, I. M. Fazal, N. Ahmed, Y. Yan, H. Huang, Y. X. Ren, Y. Yue, S. Dolinar, M. Tur, A. E. Willner, *Nat. Photonics* **2012**, *6*, 488.

[155] M. Rafayelyan, E. Brasselet, *Phys. Rev. Lett.* **2018**, *120*, 213903.

[156] T. Lin, Y. Yuan, Y. Zhou, W. Fu, H. Huang, L. Yao, F. Fan, S. Wen, *Opt. Lett.* **2019**, *44*, 2720.

[157] T. Lin, Y. Zhou, Y. Yuan, W. Fu, L. Yao, H. Huang, F. Fan, S. Wen, *Opt. Express* **2018**, *26*, 29244.

[158] M. Ono, J. Kobashi, H. Yoshida, M. Ozaki, *J. Opt. Soc. Am. B* **2019**, *36*, D20.

[159] a) D. Broer, J. Lub, G. Mol, *Nature* **1995**, *378*, 467; b) D. J. Broer, G. N. Mol, J. A. V. Haaren, J. Lub, *Adv. Mater.* **1999**, *11*, 573; c) M. Mitov, N. Dessaud, *Nat. Mater.* **2006**, *5*, 361; d) W. Hu, M. Chen, Q. Wang, L. Zhang, X. Yuan, F. Chen, H. Yang, *Angew. Chem., Int. Ed.* **2019**, *58*, 6698.

[160] M. Rafayelyan, G. Agez, E. Brasselet, *Phys. Rev. A* **2017**, *96*, 043862.

[161] J. Kobashi, H. Yoshida, M. Ozaki, *Mol. Cryst. Liq. Cryst.* **2017**, *646*, 116.

[162] J. Kobashi, H. Yoshida, M. Ozaki, *Sci. Rep.* **2017**, *7*, 16470.

[163] a) Q. Wang, E. T. F. Rogers, B. Gholipour, C. M. Wang, G. Yuan, J. Teng, N. I. Zheludev, *Nat. Photonics* **2016**, *10*, 60; b) H. S. Ee, R. Agarwal, *Nano Lett.* **2016**, *16*, 2818; c) S. C. Malek, H. S. Ee, R. Agarwal, *Nano Lett.* **2017**, *17*, 3641; d) X. Yin, T. Steinle, L. Huang, T. Taubner, M. Wuttig, T. Zentgraf, H. Giessen, *Light: Sci. Appl.* **2017**, *6*, e17016; e) J. Li, S. Kamin, G. Zheng, F. Neubrech, S. Zhang, N. Liu, *Sci. Adv.* **2018**, *4*, eaar6768; f) A. She, S. Zhang, S. Shian, D. R. Clarke, F. Capasso, *Sci. Adv.* **2018**, *4*, eaap9957; g) P. Yu, J. Li, X. Li, G. Schütz, M. Hirscher, S. Zhang, N. Liu, *ACS Nano* **2019**, *13*, 7100.

[164] a) S. S. Choi, S. M. Morris, W. T. S. Huck, H. J. Coles, *Adv. Mater.* **2009**, *21*, 3915; b) L. Zhang, L. Wang, U. S. Hiremath, H. K. Bisoyi, G. G. Nair, C. V. Yelamaggad, A. M. Urbas, T. J. Bunning, Q. Li, *Adv. Mater.* **2017**, *29*, 1700676; c) Y. C. Hsiao, Z. H. Yang, D. Shen, W. Lee, *Adv. Opt. Mater.* **2018**, *6*, 1701128; d) S. Tokunaga, Y. Itoh, H. Tanaka, F. Araoka, T. Aida, *J. Am. Chem. Soc.* **2018**, *140*, 10946.

[165] K. Yin, Y. H. Lee, Z. He, S. T. Wu, *Opt. Express* **2019**, *27*, 5814.

[166] K. Yin, Y. H. Lee, Z. He, S. T. Wu, *J. Soc. Inf. Disp.* **2019**, *27*, 232.

[167] Y. Huang, Y. Zhou, C. Doyle, S. T. Wu, *Opt. Express* **2006**, *14*, 1236.

[168] a) Y. Inoue, H. Yoshida, H. Kubo, M. Ozaki, *Adv. Opt. Mater.* **2013**, *1*, 256; b) M. Mohammadimasoudi, J. Beeckman, J. Shin, K. Lee, K. Neyts, *Opt. Express* **2014**, *22*, 19098; c) S. Wood, J. Fells, S. Elston, S. Morris, *Macromolecules* **2016**, *49*, 8643.

[169] B. A. Kowalski, V. P. Tondiglia, K. M. Lee, D. R. Evans, T. J. White, M. S. Mills, *Opt. Express* **2019**, *27*, 16571.

[170] R. Chen, Y. H. Lee, T. Zhan, K. Yin, Z. An, S. T. Wu, *Adv. Opt. Mater.* **2019**, *7*, 1900101.

[171] a) C. L. Van Oosten, C. W. Bastiaansen, D. J. Broer, *Nat. Mater.* **2009**, *8*, 677; b) T. J. White, R. L. Bricker, L. V. Natarajan, N. V. Tabiryan, L. Green, Q. Li, T. J. Bunning, *Adv. Funct. Mater.* **2009**, *19*, 3484; c) Q. Li, Y. Li, J. Ma, D. K. Yang, T. J. White, T. J. Bunning, *Adv. Mater.* **2011**, *23*, 5069; d) W. Feng, D. J. Broer, D. Liu, *Adv. Mater.* **2018**, *30*, 1704970; e) T. Orlova, F. Lancia, C. Loussert, S. Iamsaard, N. Katsonis, E. Brasselet, *Nat. Nanotechnol.* **2018**, *13*, 304.

[172] P. Chen, L. L. Ma, W. Hu, Z. X. Shen, H. K. Bisoyi, S. B. Wu, S. J. Ge, Q. Li, Y. Q. Lu, *Nat. Commun.* **2019**, *10*, 2518.

[173] H. Rubinsztein-Dunlop, A. Forbes, M. V. Berry, M. R. Dennis, D. L. Andrews, M. Mansuripur, C. Denz, C. Alpmann, P. Banzer, T. Bauer, E. Karimi, L. Marrucci, M. Padgett, M. Ritsch-Marte, N. M. Litchinitser, N. P. Bigelow, C. Rosales-Guzmán, A. Belmonte, J. P. Torres, T. W. Neely, M. Baker, R. Gordon, A. B. Stilgoe, J. Romero, A. G. White, R. Fickler, A. E. Willner, G. Xie, B. McMorran, A. M. Weiner, *J. Opt.* **2017**, *19*, 013001.

[174] a) A. Chong, W. H. Renninger, D. N. Christodoulides, F. W. Wise, *Nat. Photonics* **2010**, *4*, 103; b) K. Toyoda, F. Takahashi, S. Takizawa, Y. Tokizane, K. Miyamoto, R. Morita, T. Omatsu, *Phys. Rev. Lett.* **2013**, *110*, 143603; c) J. Ni, C. Wang, C. Zhang, Y. Hu, L. Yang, Z. Lao, B. Xu, J. Li, D. Wu, J. Chu, *Light: Sci. Appl.* **2017**, *6*, e17011; d) J. Ni, Z. Wang, Z. Li, Z. Lao, Y. Hu, S. Ji, B. Xu, C. Zhang, J. Li, D. Wu, J. Chu, *Adv. Funct. Mater.* **2017**, *27*, 1701939.

[175] a) H. Kikuchi, M. Yokota, Y. Hisakado, H. Yang, T. Kajiyama, *Nat. Mater.* **2002**, *1*, 64; b) Y. Hisakado, H. Kikuchi, T. Nagamura, T. Kajiyama, *Adv. Mater.* **2005**, *17*, 96; c) T. H. Lin, Y. Li, C. T. Wang, H. C. Jau, C. W. Chen, C. C. Li, H. K. Bisoyi, T. J. Bunning, Q. Li,

**ADVANCED
SCIENCE NEWS**

www.advancedsciencenews.com

**ADVANCED
MATERIALS**

www.advmat.de

Adv. Mater. **2013**, *25*, 5050; d) S. S. Gandhi, L. C. Chien, *Adv. Mater.* **2017**, *29*, 1704296.

[176] a) C. W. Chen, C. T. Hou, C. C. Li, H. C. Jau, C. T. Wang, C. L. Hong, D. Y. Guo, C. Y. Wang, S. P. Chiang, T. J. Bunning, I. C. Khoo, T. H. Lin, *Nat. Commun.* **2017**, *8*, 727; b) Z. G. Zheng, C. L. Yuan, W. Hu, H. K. Bisoyi, M. J. Tang, Z. Liu, P. Z. Sun, W. Q. Yang, X. Q. Wang, D. Shen, Y. Li, F. Ye, Y. Q. Lu, G. Li, Q. Li, *Adv. Mater.* **2017**, *29*, 1703165.

[177] R. P. Lemieux, *Chem. Soc. Rev.* **2007**, *36*, 2033.

[178] J. Xiang, Y. Li, Q. Li, D. A. Paterson, J. M. Storey, C. T. Imrie, O. D. Lavrentovich, *Adv. Mater.* **2015**, *27*, 3014.

[179] a) F. Lin, Z. Zhu, X. Zhou, W. Qiu, C. Niu, J. Hu, K. Dahal, Y. Wang, Z. Zhao, Z. Ren, D. Litvinov, Z. Liu, Z. M. Wang, J. Bao, *Adv. Mater.* **2017**, *29*, 1604453; b) F. Lin, G. Yang, C. Niu, Y. Wang, Z. Zhu, H. Luo, C. Dai, D. Mayerich, Y. Hu, J. Hu, X. Zhou, Z. Liu, Z. M. Wang, J. Bao, *Adv. Funct. Mater.* **2018**, *28*, 1805255; c) B. Tian, W. Lin, P. Zhuang, J. Li, T. M. Shih, W. Cai, *Carbon* **2018**, *131*, 66.

[180] a) T. Z. Shen, S. H. Hong, J. K. Song, *Nat. Mater.* **2014**, *13*, 394; b) L. He, J. Ye, M. Shuai, Z. Zhu, X. Zhou, Y. Wang, Y. Li, Z. Su, H. Zhang, Y. Chen, Z. Liu, Z. Cheng, J. Bao, *Nanoscale* **2015**, *7*, 1616.

[181] D. Rossi, J. H. Han, W. Jung, J. Cheon, D. H. Son, *ACS Nano* **2015**, *9*, 8037.

[182] a) Y. J. Liu, G. Y. Si, E. S. P. Leong, N. Xiang, A. J. Danner, J. H. Teng, *Adv. Mater.* **2012**, *24*, OP131; b) D. Franklin, Y. Chen, A. Vazquez-Guardado, S. Modak, J. Boroumand, D. Xu, S. T. Wu, D. Chanda, *Nat. Commun.* **2015**, *6*, 7337; c) J. Sautter, I. Staude, M. Decker, E. Rusak, D. N. Neshev, I. Brener, Y. S. Kivshar, *ACS Nano* **2015**, *9*, 4308; d) J. Bohn, T. Bucher, K. E. Chong, A. Komar, D. Y. Choi, D. N. Neshev, Y. S. Kivshar, T. Pertsch, I. Staude, *Nano Lett.* **2018**, *18*, 3461; e) Z. Shen, S. Zhou, S. Ge, W. Duan, P. Chen, L. Wang, W. Hu, Y. Lu, *Opt. Lett.* **2018**, *43*, 4695; f) A. M. Shaltout, V. M. Shalaev, M. L. Brongersma, *Science* **2019**, *364*, eaat3100.